Uppsats för licentiatexamen

TUNNELING THROUGH A SINGLE QUENCH-CONDENSED BISMUTH CLUSTER

Andrey Danilov

CHALMERS | GÖTEBORGS UNIVERSITET

Institution för mikroelektronik och nanovetenskap
Chalmers tekniska högskola och Göteborgs universitet
Göteborg 2000

Tunneling through a single quench-condensed bismuth cluster.

ANDREY DANILOV

Technical report no. GIPR-355
Department of Microelectronics and Nanoscience
Chalmers University of Technology and Göteborg University
SE-412 96 Göteborg
Sweden
Telephone + 46 (0)31 772 1000

ISSN 0280-2872
Chalmersbibliotekets reproservice och
Fysiksektionens reproservice
Göteborg, Sweden 2000

PREFACE

The progress of miniaturisation in conventional electronics will eventually hit the limit where new physical principles for basic electronic devices will be necessary. Such a device - a Single Electron Transistor (SET) - has already emerged in contemporary low temperature physics. This device is making the use of electrostatic energy needed to charge a small island separated by two tunneling barriers from the contact leads.

The advantage of such a device is that the smaller the island size, the better the transistor performance. Current nanofabrication facilities allow reliable nanofabrication in the scale of 100 nm, this limits the SET operation temperatures to the millikelvin range. However, a reduction of the island size to (1-2) nm would allow its operation at room temperature. We have developed a fabrication method which allows to produce such devices and we successfully used this method to implement a room temperature operating SET.

Using oblique evaporation through conventional electron-beam lithographic masks as the sample resistance was measured *in situ*, we defined constrictions with widths and lengths of about 5 nm in thin (1-3) nm granular films. The tunneling conductivity through a limited network of metallic grains was studied. The nominal film thickness in the constriction could be varied stepwise in the range (2-5) nm by *in situ* film depositions, changing the grain size and the configuration of the tunneling paths. As the film thickness was increased, the multigrain structure was replaced by a SET geometry with a single island dominating in the current transport.

Best results were achieved when the method was applied to quench-condensed (QC) films. Despite the random nature of cluster formation in QC films, samples with periodic gate dependency and well-formed Coulomb diamonds were routinely obtained in every experimental run.

Sample preparation is just sketchily described in the thesis, for future reference look in appended papers:

- The fabrication method and room temperature SET are presented in appended papers ## 1-2;
- For method application to a quench-condensed films look in appended papers ## 3-4;

In this thesis we will focus on two subjects:

- An unexpected manyfold increase of SET conductance at temperatures below ~ 7 K. This effect is attributed to a phase transition in bismuth clusters of a new type, with the cluster shape as the order parameter.

- Tunneling spectroscopy data, taken on a single quench-condensed bismuth cluster placed in a well-defined SET geometry. Interpretation of these data indicates that surface-localised states dominate in the current transport.

We would like to stress that this is research in progress, with many aspects yet to be understood (and to be measured, too). But we believe that already these preliminary spectroscopy data together with the phase transition, likely observed in our cluster electronic system, lead to remarkable conclusions:

The quench-condensed clusters are not frozen, their shape is self-adjusted to minimise the electronic energy. As a result, a shell structure is formed in an energy spectrum . The energy gap near the Fermi energy in a shell spectrum makes cluster electronic properties rather different from those of a bulk metal.

Contents

1. FABRICATION METHOD

1.1. Quench-Condenced Films as a Source of Clusters

Metallic films prepared by vapor deposition on a cold (4-10) K substrate - quench-condensed (QC) films - have been extensively used as model objects to study the effect of disorder on electron localization [1,2] and superconductivity [3]. Films prepared on chemically neutral substrates are believed to consist of small islands, although there is no clear picture of the island formation in extreme conditions where thermally activated diffusion is frozen [4,5]. Until recently, the film structure was deduced from macroscopic electron transport measurements, providing an information that is averaged over the whole sample. No direct measurements of the local transport properties have yet been performed.

After initial experiments with macroscopic QC films [4,5] we realised that confining a sample geometry to a nanometer-sized constriction will provide valuable information on film morphology and transport properties at a microscopic scale, i.e. below the typical cluster size in a film near percolation threshold.

As the structure of QC films is metastable, it can only be studied *in situ*. Recently, the morphology of these films has been studied by a cryogenic STM [6]. Fig. 1, reproduced from Ref. [6], shows STM topography images of QC gold film in the thickness range in which the film first became electrically continuos.

This was the first study of the microscopic structure of QC films. An unusual film growth scenario was found. The island formation happens suddenly by an avalanche in the amorphous precursor layer. The existence of islands in QC films was confirmed experimentally and charging energies as high as 0.2 eV were reported, indicating the presence of very small islands. However, an STM study does not provide information on the local transport. A macroscopic thin film built from such small clusters would be insulating.

1.2. Angle Deposition

The main obstacle to using electron-beam masks down to 10 nm feature size is their poor reproducibility at this level, at least, under ordinary laboratory conditions. We overcame this drawback by tuning the effective size of the mask during the process of sample fabrication. Angle deposition was used to reduce the effective width of the constriction; *in situ* sample conductance measurements helped to find the proper angle when the constriction is just open (see Fig. 2).

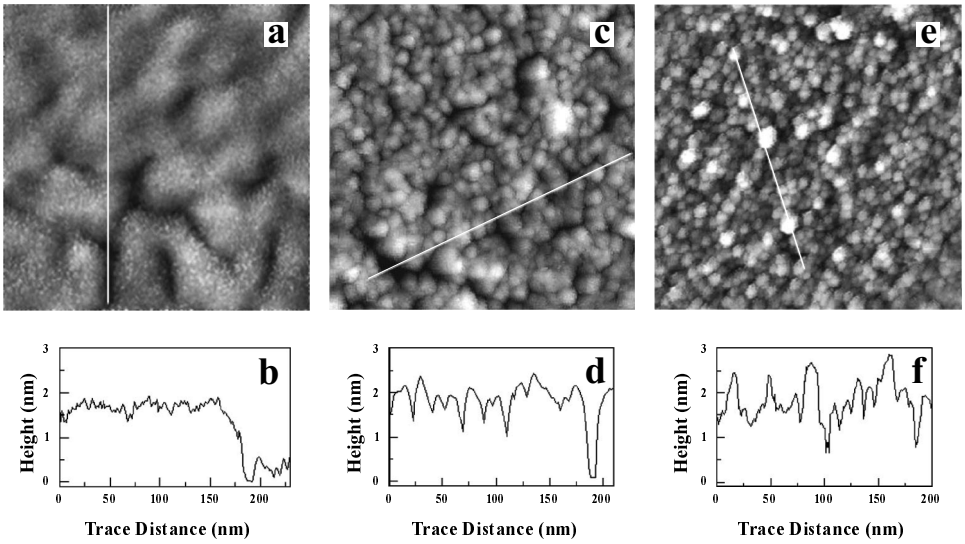

Fig. 1. In situ STM images of Au films with increasing thickness deposited on a highly oriented pyrolitic graphite substrate at 4 K. The full scale height range from black to white is 2 nm for all images. The film thicknesses and scan areas are **a**- $d = 1.6 \pm 0.1$ nm and 233×233 nm, **c**- $d = 1.8 \pm 0.1$ nm and 210×210 nm and **e**- $d = 2.2 \pm 0.1$ nm and 228×228 nm. The corresponding line scans are displayed in **b**, **d**, and **f**. Note the exaggerated height scale. From Ekinchi *et al.* [6].

We incremented a tilt angle step by step, widening the gap, and after each step in tilt angle we deposited a test metallic layer with a thickness $2 \times d_{\mathrm{C}}$ and checked the sample conductivity to determinine if the effective constriction in the mask was opened (d_{C} is a conductivity onset thickness). All further depositions to form the transistor occured at this angle,where the mask is just open. The effective width of the mask for the first conductive sample did not exceed the nominal value of step in the opening of the constriction, which was 10 nm.

The minimum step size was limited by the danger of closing the mask by the deposited material. To reduce this effect we used a metal with low d_{C}. In a number of experiments we have successfully tried a step size of 5 nm. For future details of nanofabrication procedure look in appended papers ## 1-4 (Refs. [7–10]).

The first conductive sample has a simple geometry: relatively thick (6-8) nm closely spaced low resistive electrodes, formed in the process of finding a proper tilt angle (see Fig. 2), were bridged by a narrow network of metallic

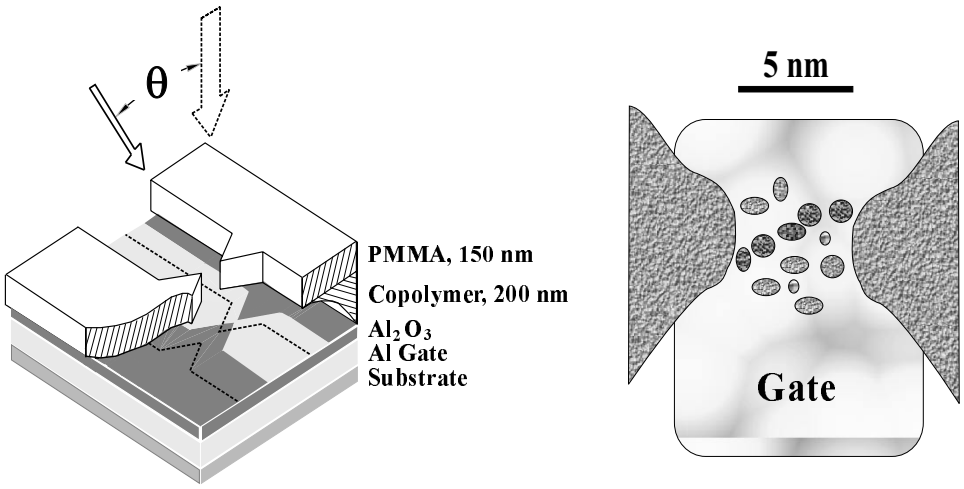

Fig. 2. **Left**: reduction of the constriction area as a result of tilt deposition. Substrate - thermally oxidized silicon wafer. **Right**: Resulting device geometry: a few grain network in a 5×5 nm^2 constriction between two self-aligned macroscopic leads. The wire-frame contour (dashed line) shows the orthogonal projection of a mask onto a substrate. This will be the result of a normal deposition.

clusters.

We studied the evolution of the electrical properties of the sample as a function of film thickness in the constriction. After each small increment of film thickness we took extensive measurements of the current-voltage characteristics at different gate voltages. Thus, in one experimental run, more than 30 different samples were prepared and characterized.

For QC bismuth films d_C, and therefore, the typical cluster size, is (1-2) nm. In the constriction of 10 by 10 nm one can imagine a maximum of 4 by 4 clusters with the typical size of 2 nm. Futher depositions increase the typical cluster size thus reducing the number of clusters in a constriction.

This evolution brings us to samples with almost perfect Coulomb diamonds and regular gate dependence - see Fig. 2 in appended paper #3 and Fig. 2 in appended paper #4. They correspond to the geometry of Single Electron Transistor, with a single grain separated by tunneling barriers from two metallic electrodes. All tunneling spectroscopy data discussed futher were collected in this well-defined geometry.

2. SINGLE ELECTRON TRANSISTOR BUILT AROUND A CLUSTER OF QUENCH-CONDENCED BISMUTH

2.1. Coulomb Blockade: Elementary Introduction

A SET transistor is a *small* grain coupled to macroscopic electrodes - Source and Drain, via two *tunneling contacts*.

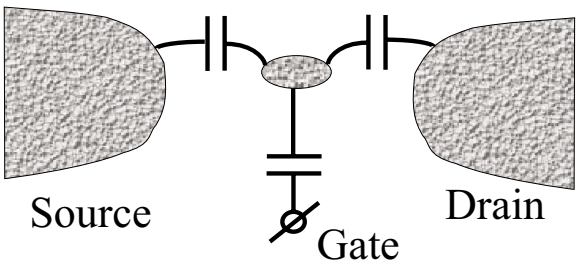

Fig. 3. A sketch of a Single Electron Transistor. A small grain is coupled to macroscopic leads via two tunnelling barriers.

The *tunneling contact*, in the simplest case, is just a vacuum gap a few Ångströms wide. An electron has some probability to jump through a gap. Before the jump the electron is on one side of the barrier and after the jump on the other. Thus, at any time, the grain has some integer number n of electrons, and the grain charge is ne, where e is an electron charge.

If the grain is *small*, say, ~ 2 nm, then the grain capacitance is about $C \sim 10^{-18}$ F, and just a single additional electron will raise the grain potential by $V_{\rm C} = e/C \sim 0.1$ V. It means that no other electron can jump into grain, and no current will pass through, if the voltage applied to the tunneling gap is less than $V_{\rm C}$. This is schematically shown in Fig. 4a.

Applying a positive potential to a third electrode - a Gate, we can make the grain more attractive for electrons. At some gate voltage, as illustrated in Fig. 4c, the transistor will be open even at zero Source-Drain voltage.

What will happen if we will make a grain even more attractive for electrons? Then the jump in will still be possible, but the jump out will be forbidden, and the transistor will be closed again - see Fig. 4e.

But, at a still more positive gate potential, the configuration with $n = 2$ additional electrons on the grain will have the same energy as one with $n = 1$. At that moment, transistor will be open at zero Source-Drain voltage again - see Fig. 4g.

Resume: sometimes we need some Source-Drain voltage to push an electron in (Fig. 4b), and sometimes to pull it out (Fig. 4f). Only if the

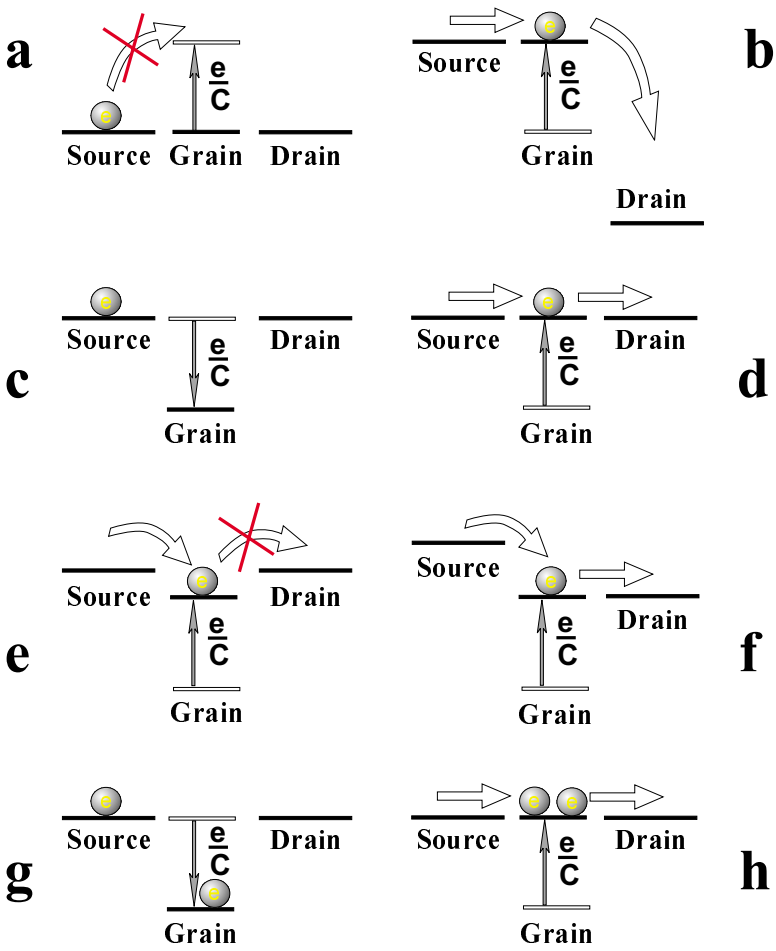

Fig. 4. SET transistor at different Gate voltages.

gate potential is exactly tuned to overcome the charging effect, a transistor is open at zero bias voltage.

At fixed bias voltage V the Source-Drain current I is periodically modulated with a gate potential V_{G}. An $I(V)$ curves have some zero-current region around $V = 0$ - a "Coulomb gap". This gap is periodically squeezed to zero with V_{G}. A more sophisticated analysis (see section 3.1.) shows that on a $V - V_{\mathrm{G}}$ plane no-current areas form rhombs - this is a so-called "diamond structure".

Illustrative experimental data are presented in Fig. 5 - see the next section.

2.2. Anomalous Temperature Dependence

In this section we will discuss the measurements of tunneling through single clusters of an amorphous quench-condensed (QC) bismuth film in a single-electron transistor geometry. Tunneling barriers, separating the central island of these transistors from the thin film electrodes, appeared naturally during the QC film growth. Electrostatic gates, made of oxidized aluminum, had been prepared in advance. They allowed tuning of the number of electrons on the island. The smallest cluster we managed to catch and study was about 3 nm in diameter.

The samples were studied at different temperatures, and we systematically observed an increase of the sample transparency, as the temperature was lowered. The data for two most documented samples are presented in this section.

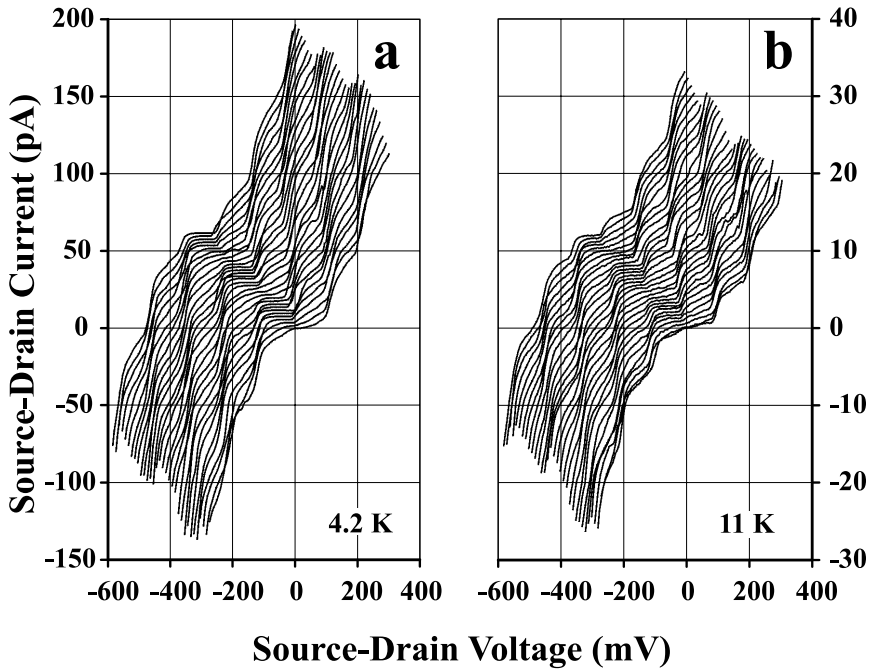

Fig. 5. **a**,**b** - Two sets of $I(V)$ curves for the sample #1 taken at different gate voltages equally spaced in the region from -900 mV to -280 mV for two temperatures: below and above the transition. Three gate periods are shown from 21 measured. These curves are displaced in vertical and lateral directions for clarity. Estimated cluster radius ~ 4 nm.

For sample #1, around $T \sim 8$ K we observed a reversible transition between two states with up to 5 times enhanced conductivity at low temperature, as it is shown in Fig. 5ab. The total charging energy of the transistor, estimated from the size of Coulomb diamonds $E_{\rm C} = 35$ meV[1]. Figures 6a-c show the effect of temperature in more details. We can see that not only the sample conductance in the open state (Fig. 6c), but also the asymptotic behavior at high bias is changed by a factor of 5 (Fig. 6b). Fig. 6a shows the current variation with temperature at different steps of the Coulomb staircase for the gate voltage corresponding to the closed state of transistor. These data demonstrate that the effect of temperature saturates at 4.2 K and 11 K for this sample. It is clear that the temperature does not activate current in the closed state (as $T \ll E_{\rm C}$), but causes a pronounced rise in current at the Coulomb steps. Note that Fig. 6b indicates that temperature variation did not change the charge distribution around the grain.

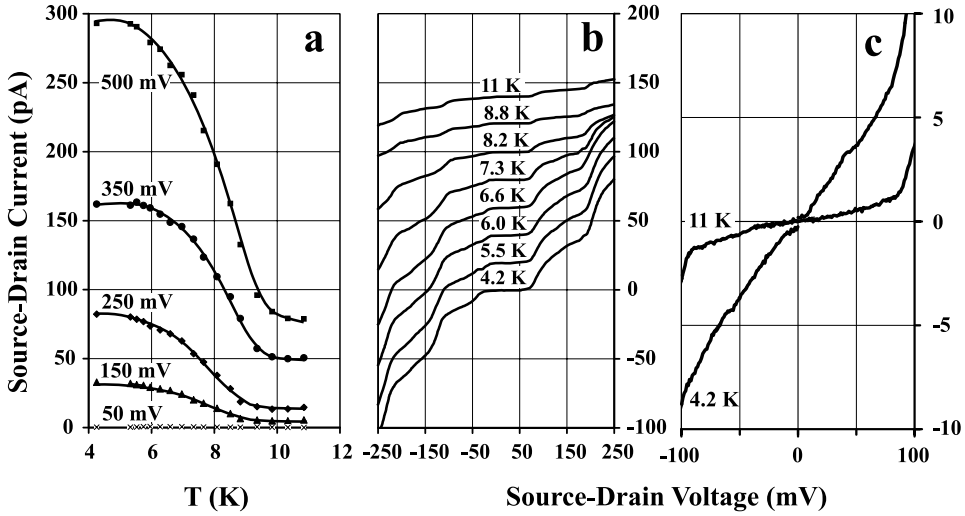

Fig. 6. The closed state at the gate voltage 0 mV: **a** - temperature dependence of a tunneling current at different biases, **b** - $I(V)$ curves taken at different temperatures. Curves are shifted for clarity. Note a constant offset charge. **c** - open state of the transistor.

[1] A fit to the orthodox model for sample #1 gives the following parameters: $C_1 = 4.5 \times 10^{-19}$ F; $C_2 = 13.4 \times 10^{-19}$ F; $C_{Gate} = 5.3 \times 10^{-19}$ F; $C_\Sigma = C_1 + C_2 + C_{Gate} = 2.3 \times 10^{-18}$ F - the same for 4 K and 11 K.

A similar temperature dependence was found for sample #2, with a charging energy of 93 meV[2] (See Fig. 7). In Fig. 7b we can also see a 5-fold increase of current around $T \sim 7$ K. The voltage scale of the effect (500 mV) allows to exclude superconductivity in the grain as a possible reason for the change of the sample characteristics. For the second sample we have determined the critical temperature of the superconducting transition in the leads by two point measurements. The result of these measurements is presented in Fig. 8b. One can see a relatively sharp transition at 3 K, well beyond the interesting region. A low critical temperature of the leads is not surprising, taking into account the thickness dependence of T_c in thin QC bismuth films[3]. These data exclude the superconducting transition in the leads as a possible reason for the observed temperature dependence.

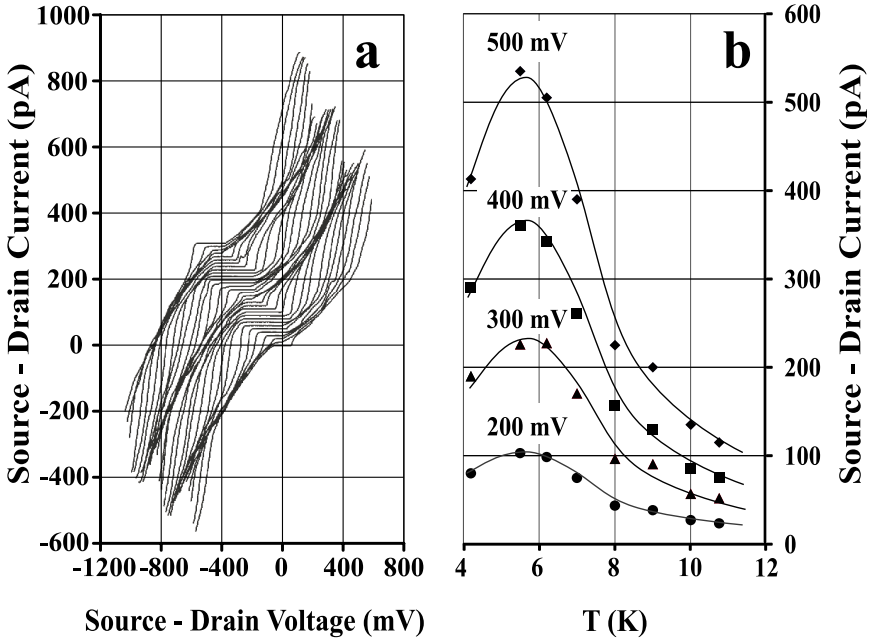

Fig. 7. Data for sample #2: **a** - A set of $I(V)$ curves taken at different gate voltages equally spaced in the region ± 1100 mV at 4.2 K. Two gate periods are shown from 4 measured. **b** - temperature dependence of the tunneling current at different biases for the open state of the transistor. Estimated cluster radius ~ 1.5 nm.

[2] A fit to the orthodox model for sample #2 gives the following parameters: $C_1 = 2.3 \times 10^{-19}$ F; $C_2 = 4.6 \times 10^{-19}$ F; $C_{Gate} = 1.7 \times 10^{-19}$ F; $C_\Sigma = 8.6 \times 10^{-19}$ F.

[3] Lead sheet resistance was about 1 k$\Omega/\Box$.

An additional 1.5 Å of evaporated metal attached the central island to one of the leads, leaving just one tunneling gap in the constriction. There was no gate dependence for this successor of sample #2. Apparently, at this moment the resistance of one of the tunneling junction became comparable to the quantum conductance, and the grain effectively merged with the electrode. The current-voltage characteristic for a single tunneling gap is shown in Fig. 8a. All data for different gate voltages and different temperatures were close to this curve within experimental accuracy. There was no temperature dependence for all other samples that followed this one, and the remaining tunneling gap width decreased linearly with the deposited material as we could see from the exponential drop of the sample resistance as a function of average film thickness.

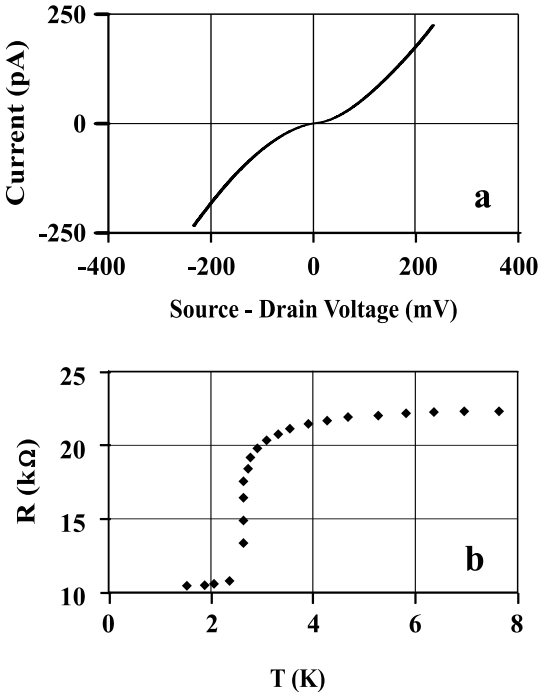

Fig. 8. **a** - an $I(V)$ curve of a single tunneling gap. **b** - superconducting transition in the leads.

From a Coulomb energy of 93 meV we can estimate the cluster radius $R_C \approx 1.5$ nm. This gives about 400 bismuth atoms and 2000 valence electrons in the cluster. We believe that cluster phenomena become important in our samples and are responsible for the observed anomalies.

2.3. Interpretation: Phase Transition in Cluster

The observed temperature dependence does not resemble one that could be expected neither from the classical orthodox Coulomb blockade[11,12] nor from quantum Coulomb blockade[13]. In a classical orthodox theory the increase of temperature activates tunneling events in the region of Coulomb blockade and smears out Coulomb staircases. In the quantum case zero bias conductivity in the open state of a transistor increases when the temperature is lowered. Moreover, any finite bias destroys resonant transparency. Both quantum and classical pictures predict that asymptotic conductance at high bias limit does not change with the temperature as it is determined by temperature independent tunneling transparencies. In our experiments, a large-scale asymptotic conductance up to bias voltages of $(500-750)$ mV was reversibly affected by the temperature variation in a very moderate window $(4-8)$ K. The temperature dependence disappears for a single gap separating two macroscopic leads. This observation confirms that barrier transparencies do not depend on temperature. The presence of at least one grain in a transport chain is crucial for the observed effect. Structures with more than one grain in the constriction demonstrated qualitatively similar, though less pronounced temperature dependence. We would like to emphasize that any network built with any number of classical single electron devices could not explain the observed temperature dependence.

Of course, the constriction size that we achieved in the described experiments is extremely small and coherent effects must play important role in the transport. At the moment, we do not see how quantum nature of the electron transport through the grain will survive on the huge voltage scale observed experimentally.

The natural way to explain this effect is a simple variation of the tunneling barrier width with the temperature. A mechanical reduction of the tunneling gap seems to be very attractive, as it might explain the increased transparency at high voltages. It is not observed in the case of a single tunneling barrier, so it must be caused by the presence of the grain. Any grain distortion would lead to the observable change of the tunneling barrier transparency[4].

We believe that the reason for such a distortion is a phase transition in

[4]Below 10 K the electronic contribution to the specific heat starts to dominate, and the linear thermal expansion $\frac{\Delta R}{R} \approx \frac{2}{9B} c^{\mathrm{el}} T$ (B is the bulk modulus and c^{el} is the electron specific heat). For a free electron model it can be estimated as $\frac{\pi^2}{6}\left(\frac{k_{\mathrm{B}}T}{E_{\mathrm{F}}}\right)^2$ (k_{B} is a Boltzmann's constant and E_{F} is a Fermi energy) and is negligible - see Ref. [14], Chap. 25. Moreover, the effect can not be reduced to a trivial thermal expansion because it is not observed for a single tunneling gap separating two macroscopic leads.

the grain, occurring around 8 K - see Fig. 9.

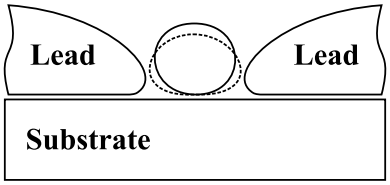

Fig. 9. As a result of a phase transition, a cluster tends to restore a spherical symmetry at high temperatures. This leads to increasing tunneling gaps above the transition temperature.

Indeed, a similar phase transition in a free metallic cluster was predicted in Ref. [15]. A well-established picture of shells in free metallic clusters[16,17] predicts that the ground state of a cluster with unfilled electron shells is not spherical[5]. However, at a finite temperature, thermal perturbations of the electron density recover the spherical symmetry, and there is a phase transition associated with this scenario where shape plays the role of the order parameter. Despite the relatively high electron energies involved, the critical temperature T_c of the transition is rather low and falls down, as fast as the number of electrons in a cluster N increases: for the cluster with $N = 13$ potassium atoms $T_c \sim 1400$ K while for $N = 75$ it is already around 200 K. The T_c is proportional to the square of Wigner-Seitz radius r_S. It is a factor of two smaller for amorphous bismuth, as compared to potassium[6], lowering the T_c even further. Therefore, we would expect T_c in the range of 10 K, for bismuth clusters with sizes $N \sim 10^3$. Unfortunately, at such low temperatures, the estimation of the electron-phonon interaction, used in the theory, becomes too crude. In addition, there are indications that in small clusters at low temperature the electron-electron exchange interaction becomes important[18,19]. All these circumstances were neglected in the theory. Thus, a quantitative application of the theory from Ref. [15] to our results is not possible. However, it provides a clear picture of the physical situation achieved in our experiments. For small clusters like those measured in our experiments, the electron contribution to the energy is dominant and the electronic system rules the behavior of a small cluster[7].

[5] We will discuss the shells effects in details later in section 6.1.

[6] A free electron model gives $r_S = 2.08$ Å for sodium and $r_S = 1.19$ Å for bismuth (assuming 5 free electrons per one bismuth atom) - see Ref. 14, Chap. 1.

[7] There are indications that electron shell structure determines abundance spectra even in open metallic nanowires at low temperatures - see Ref. [20]

Tunneling in a lateral geometry allows the detection of extremely small variations of the cluster size. The expected effect of the shape distortion, however, is not small as it equals the ground state cluster deformation and reaches 1 Å for a cluster with $N \sim 10^2$ - see Ref. [21]. The change of transparency, observed in our measurements, can be accounted for by a 0.3 Å variation of the tunneling gap. For a cluster with a closed electron shell, the ground state is perfectly spherical and so the transition temperature goes to zero. Since the probability to meet a cluster with the completely filled shell is virtually zero, it is not surprising that the effect is so robust and reproducible. We have to say, however, that the transition temperature was higher for the cluster from sample #1 with lower charging energy (and bigger N). Possibly, this cluster was closer to the filled shell configuration, than the cluster from the sample #2.

Let us discuss the role of substrate, as theoretical results are related to free clusters in vacuum. The characteristic feature of our experiments is that most part of a cluster surface in a QC film remains free. A cluster experiences relatively weak Van-der-Waals interaction with the chemically inert substrate. Therefore the fact that our cluster is suspended should not disturb much a picture of electron shells and the scenario of a phase transition described in Ref. [15]. Then, the substrate influence on the cluster can be treated as an external field in the theory of phase transitions[22]. The result is that a phase transition survives in the external field, though with a lower critical temperature.

3. SPECTROSCOPIC MEASUREMENTS OF DISCRETE ELECTRONIC STATES IN A SINGLE ELECTRON TRANSISTOR GEOMETRY

Mesoscopic metallic systems, that are so small that the splitting between discrete single-electron levels due to spatial confinement exceeds the temperature have recently become accessible to experiments. Connecting such a small system to a macroscopic lead electrode via a metallic contact will, of course, destroy the energy quantization. Thus, the tunneling links are the only way to arrange a non-destructive measurement circuit.

A small grain, with charging energy exceeding the temperature[8], coupled to macroscopic leads via tunneling contacts, is nothing but a Single Electron Tunneling (SET) transistor. So the tunneling spectroscopy in a SET geometry is the most straightforward way to study the energy spectra in a mesoscopic samples.

This is a hot topic in modern low temperature physics, and in this section we will present an elementary introduction into the subject, followed by a review of recent publications in this field.

3.1. Spectroscopy in a SET geometry: Elementary Introduction

To discuss the basic idea of spectroscopic measurements in a SET geometry we will start from a sketch of a SET presented in Fig. 10.

For simplicity, we will assume an asymmetric case with the left tunnelling conductance much lower than the right one. At low voltages, barrier capacitances together with the gate capacitance form a capacitance voltage divider, so the voltage applied, say, to the left gap V_1 is some linear combination of bias V and gate V_g voltages. On the other hand it means that applying V and V_g in some special linear proportion one can keep, say V_1 voltage constant and bias the main tunneling gap only.

Indeed, if the grain is charged by n electrons then at equilibrium

$$\begin{aligned} q_1 &= \frac{C_1}{C_\Sigma}\left(-en + \left(C_2 + \frac{1}{2}C_g\right)V - C_g V_g\right), \\ q_2 &= \frac{C_2}{C_\Sigma}\left(en + \left(C_1 + \frac{1}{2}C_g\right)V + C_g V_g\right), \\ q_g &= \frac{C_g}{C_\Sigma}\left(-en - \frac{1}{2}(C_1 - C_2)V + (C_1 + C_2)V_g\right), \end{aligned} \tag{1}$$

[8] The charging energy E_C always exceeds the level splitting δE due to quantization, i.e. the condition $\delta E > k_B T$ implies also $E_C > k_B T$.

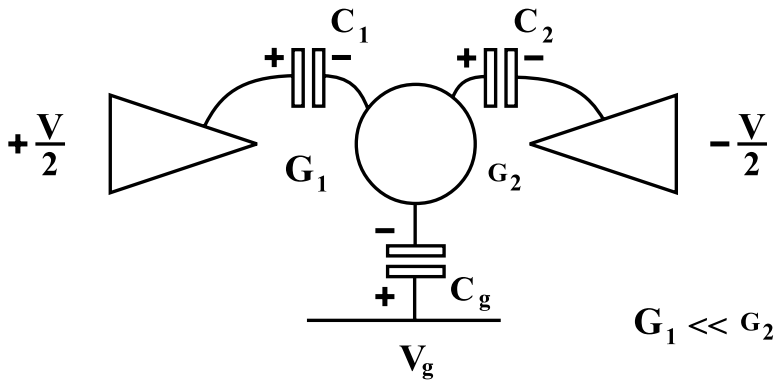

Fig. 10. Basic notations: a grain is coupled to macroscopic leads via two tunnelling barriers with conductances G_1 and G_2. The grain has capacitors C_1 and C_2 to the leads and C_g to a gate electrode.

where $C_\Sigma = C_1 + C_2 + C_g$ and charge sign convention is shown in Fig. 10.

The condition $V_2 = q_2/C_2 = const$ is equivalent to

$$\mathrm{d}q_2(V, V_g) = \frac{1}{C_\Sigma}\left(\left(C_1 + \frac{1}{2}C_g\right)\mathrm{d}V + C_g \mathrm{d}V_g\right) = 0. \qquad (2)$$

It means that the condition $\mathrm{d}V_2 = 0$ is satisfied along any line in a (V, V_g) plane with a slope

$$\frac{\mathrm{d}V_g}{\mathrm{d}V} = -\left(\frac{C_1}{C_g} + \frac{1}{2}\right), \qquad (3)$$

indicated in Fig. 11 by an arrow $V_2 = const$[9].

Along this direction only the left gap is biased, and so the cross-section of an $I(V, V_g)$ plot along this line gives essentially the $I(V)$ curve of the main tunneling gap. Of course, there is some current gap around zero bias due to Coulomb blockade, and, at higher biases, a linear $I(V)$ if a grain spectrum is continuous. But if a spectrum is quantized, an $I(V)$ curve will be stepwise, and each step on $I(V)$ will give a delta-spike on $\mathrm{d}I/\mathrm{d}V$. If the grain spectrum does not depend on gate voltage, or, more generally speaking, on electrostatic field, then it will be the same $I(V)$ curve at any cross-section, and so spectral lines will be parallel to each other and to the diamond edge.

[9]Provided the quantized grain charge ne remains constant. But for an asymmetric transistor the grain potential follows the potential of a high conducting electrode, and so the grain charge does not depend on the voltage drop V_1 along the main tunneling gap. See Appendix A for detailed theory.

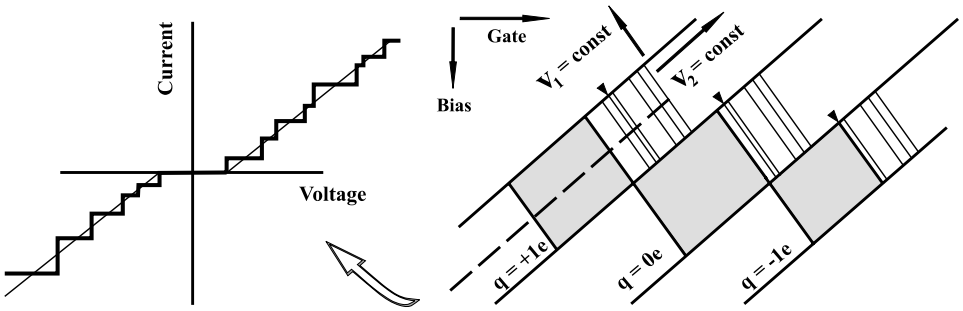

Fig. 11. Spectroscopy measurements in a SET geometry: along direction indicated by $V_2 = const$ only the main tunneling gap is biased, and so the cross-section of an $I(V, V_g)$ plot along this line gives essentially an $I(V)$ curve of the main tunneling gap.

The diamond edge marks the position of the lowest unoccupied state. If ξ_n is the first empty state in a grain charged with n electrons then in a grain charged with one additional electron ξ_n will be occupied, and the first empty energy level will be ξ_{n+1}. This is why a line marked by a triangle in Fig. 11 has a different position in spectrum for $q = -1e, q = 0e$, and $q = +1e$ ($e = +1.6 \times 10^{-19}$ C).

Note also that if the grain spectrum is quantized then the diamonds have different sizes which we will calculate below.

If the grain charge before a tunneling jump is en, then the total electrostatic energy of all network capacitancies is

$$E_{\rm Coulomb}(n) = \frac{q_1^2(n)}{2C_1} + \frac{q_2^2(n)}{2C_2} + \frac{q_g^2(n)}{2C_g} = \frac{e^2n^2}{2C_\Sigma} + BV_g^2 \quad (\text{for } V = 0). \quad (4)$$

The last term does not depend on n and will not contribute into a final result.

Because of charge redistribution after tunnelling a charge accumulated by the gate capacitance will have a new value, i. e. some charge $q_g(n+1) - q_g(n)$ will pass through the gate voltage supply, and a work ΔA produced by the power source will be

$$\Delta A = V_g\Big(q_g(n+1) - q_g(n)\Big) = -\frac{C_g}{C_\Sigma}eV_g \quad (\text{for } V = 0), \quad (5)$$

and the decrement in the electron's kinetic energy during tunnelling will be

$$\Delta K(n) = -\Big(E_{\rm Coulomb}(n+1) - E_{\rm Coulomb}(n) + \Delta A\Big) = -\frac{e^2}{C_\Sigma}\left(n + \frac{1}{2}\right) + \frac{C_g}{C_\Sigma}eV_g. \quad (6)$$

The tunnelling will be possible at zero bias voltage if for an electron with Fermi energy $E_{\rm F}$ in a lead the kinetic energy after tunnelling will be ξ_{n+1} - the energy of the lowest empty level in a grain with n electrons.

This condition is satisfied at some gate voltage V_g^n for a grain charge en and at V_g^{n-1} for a grain charge $e(n-1)$:

$$\begin{aligned} \xi_{n+1} - E_{\rm F} &= -\frac{e^2}{C_\Sigma}\left(n+\frac{1}{2}\right) + \frac{C_g}{C_\Sigma} e V_g^n, \\ \xi_n - E_{\rm F} &= -\frac{e^2}{C_\Sigma}\left(n-\frac{1}{2}\right) + \frac{C_g}{C_\Sigma} e V_g^{n-1}. \end{aligned} \tag{7}$$

Subtracting the second equation in (7) from the first one, we have for the diamond diagonal along the gate axis $V_g^n - V_g^{n-1}$

$$\frac{e^2}{C_\Sigma} + \xi_{n+1} - \xi_n = \frac{C_g}{C_\Sigma} e \left(V_g^n - V_g^{n-1}\right). \tag{8}$$

Now we know the position of the diamond corners on a gate axis from (8), and we know the slope for one pair of diamond edges from (3). For another pair a slope is given by an equation complementary to (3):

$$\frac{{\rm d}V_g}{{\rm d}V} = \left(\frac{C_2}{C_g} + \frac{1}{2}\right), \tag{9}$$

So the diamonds are completely defined, and they are presented in Fig. 12:

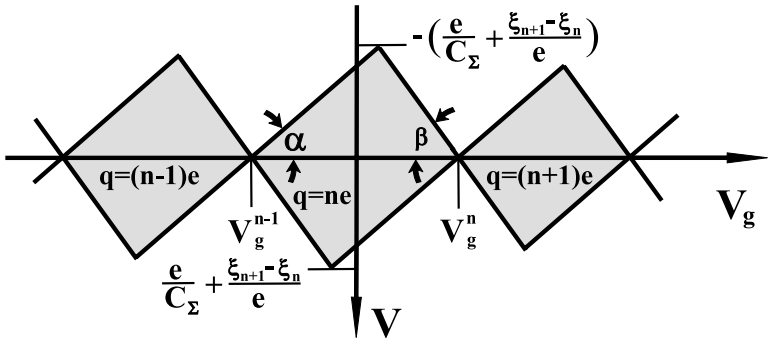

Fig. 12. Coulomb diamonds for a single grain SET having a discrete energy spectrum. Coulomb blockade is lifted when $eV_g^n = \frac{e^2}{C_g}\left(n+\frac{1}{2}\right) + \frac{C_\Sigma}{C_g}(\xi_{n+1} - E_{\rm F})$, where $E_{\rm F}$ is the Fermi energy of electrons in the leads. $\tan^{-1}\alpha = \left(\frac{C_1}{C_g} + \frac{1}{2}\right)$; $\tan^{-1}\beta = \left(\frac{C_2}{C_g} + \frac{1}{2}\right)$.

3.2. Experiments with Semiconductor Quantum Dots: Review

To observe a fine structure of an $I(V)$ curve coming from the energy levels quantization one should go down with the temperature to satisfy the condition

$$kT < \delta E, \tag{10}$$

where δE is an interlevel spacing. In fact, the condition is even stronger, as the Fermi-distribution of electrons in the leads gives the level smearing $4kT$ (full width at half maximum[23]).

This condition was first satisfied in experiments with semiconductor quantum dots (see for review [24, 25, 26] and references therein). A semiconductor quantum dot is a system based on a planar confinement applied to a two dimensional electron gas (2-DEG).

Progress in semiconductor technology in recent few years has enabled the fabrication of structures with typical lateral dimensions below 100 nm ('artificial atoms'). Due to a strong confinement of the 2-DEG in a normal direction (typically a few Å) an achivable interlevel spacing is a few meV (for a bulk sample $100 \times 100 \times 100$ nm^3 it would be 1000 times smaller). So spectral features are resolvable at temperatures below 0.1 meV or 1 K.

One of the best results in this field is presented in Fig. 13, reproduced from a paper by Kouwenhoven *et al.* [27]. Fig. 13a shows peaks in device transmissivity at zero bias versus the gate voltage. The spacing between peaks n and $n+1$ is proportional to the addition energy

$$\Delta E_n = \frac{e^2}{C_\Sigma} + \xi_{n+1} - \xi_n, \tag{11}$$

where ξ_{n+1} is the energy of the lowest unoccupied level and ξ_n is the energy of the highest occupied level (see (8)). ΔE_n is plotted versus the number of electrons in a dot in Fig. 13b.

Evolution of current peaks marking the position of levels 5, 6 and 7 with magnetic field is shown in Fig. 14b.

The electronic states are significantly modified by a magnetic field B normal to the 2-DEG plane. As the confinement area is much smaller than an interelectrode spacing, an electrostatic potential within the confinement is quadratic with a very good accuracy. The energy spectrum in a B field can be solved analytically for a dot with a 2D radial harmonic confining potential. The energy E_{nl} of a state with a radial quantum number n (=0, 1, 2, . . .) and angular momentum quantum number l (= 0, ±1, ±2, . . .) is given by

$$E_{nl} = (2n + |l| + 1)\hbar(\frac{1}{4}\omega_c^2 + \omega_0^2)^{\frac{1}{2}} - \frac{1}{2}l\hbar\omega_c, \tag{12}$$

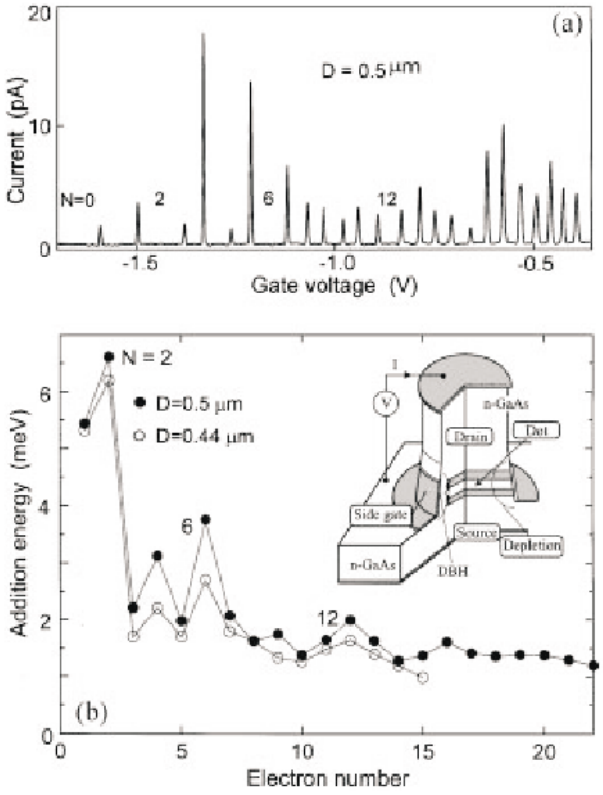

Fig. 13. **a.**- Coulomb oscillations in the current vs gate voltage at $B = 0$ T observed for a $D = 0.5$ μm dot (bias voltage $V \ll \frac{e^2}{C_\Sigma}$). **b.**- Addition energy vs electron number for two different dots with $D = 0.5$ and 0.44 μm. The inset shows a schematic diagram of the device. The dot is located between the two heterostructure barriers. (From Kouwenhoven *et al.* [27].)

where $\hbar\omega_0$ is the electrostatic confinement energy and $\hbar\omega_c$ is the cyclotron energy. Spin is neglected so each state is twofold degenerate. The resulting dependency is plotted in Fig. 14a. The dashed line in Fig. 14a marks the energy curve for the seventh and eighth electrons to illustrate that these electrons undergo transitions in their quantum numbers: (n, l) goes from (0, 2) to (0, -1) at 1.3 T and then to (0, 3) at 2 T.

An improved experimental technique in Ref. [29] resulted in data presented in Fig. 15. The Coulomb diamonds have obviously a different size, and the diamonds for $N = 2$,6, and 12 are unusually large, which correspond to filled shells. Spectral lines, running parallel to the diamond edges are also

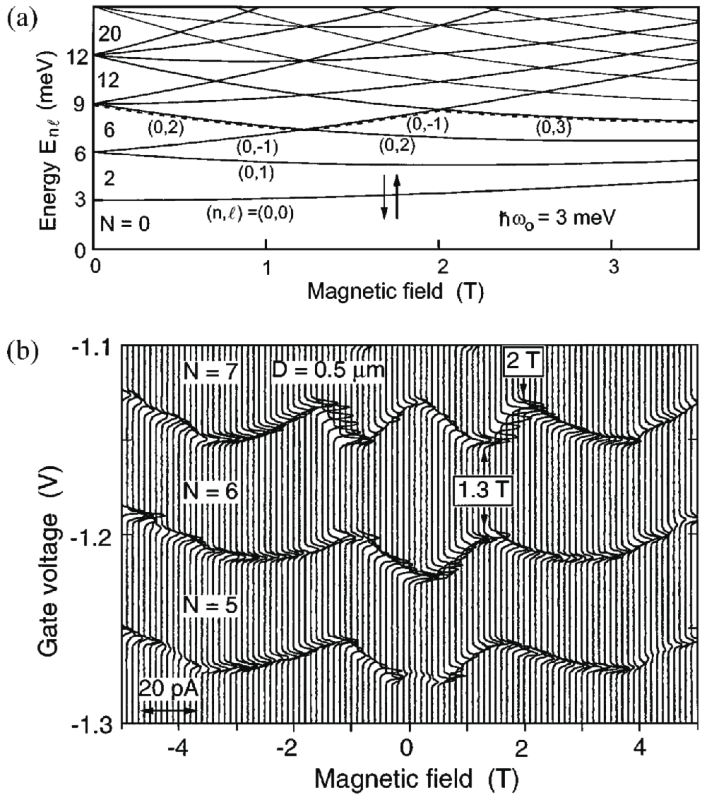

Fig. 14. **a.**-Calculated single-particle energy vs magnetic field for a parabolic potential with $\hbar\omega_0 = 3$ meV. Each state is twofold spin degenerate. The dashed line marks the lowest empty level for a dot charged with 7 electrons. **b.**- Evolution of the fifth, sixth, and seventh current peaks with B field from -5 to 5 T observed for the D = 0.5 μm dot. The original data consist of current vs gate voltage traces for different magnetic fields, which are offset and rotated by 90^o. (From Kouwenhoven *et al.* [27].)

clearly distinguishable. Note that as this transistor has two tunneling resistances approximately equal, the spectral sets, parallel to both pairs of diamond edges, have comparable intensity.

Enhanced resolution in experiments with double quantum dots allowed to observe crossings and anticrossings in the energy spectrum as a function of magnetic field[30] and to trace the crossover from molecular-like spectrum for weakly coupled double dot system to an atomic-like spectrum for strongly coupled system[31].

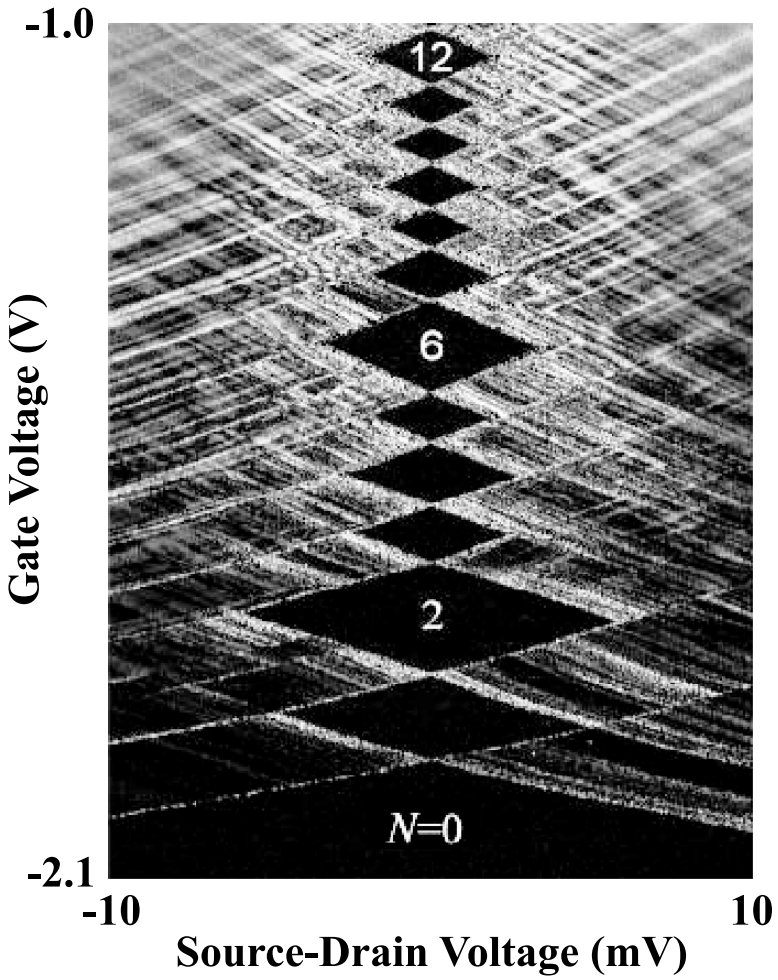

Fig. 15. Energy level spectroscopy in a SET geometry: Differential conductance $\mathrm{d}I/\mathrm{d}V$ plotted in grayscale in the (V, V_g) plane. In the black diamond-shaped regions, $\mathrm{d}I/\mathrm{d}V = 0$ as a result of Coulomb blockade. N is fixed in each of the diamond regions. The lines outside the diamonds, running parallel to the sides, identify exited states. (From Kouwenhoven *et al.* [29].)

To summarise, measurements of a non-linear $I(V)$ characteristic of a dot allows one to extract the tunnelling density of states in a confined interacting electron system. The excited levels result in distinct current steps in the $I(V)$ characteristic. Measurement of the biases corresponding to the peaks in the differetial conductance $\mathrm{d}I/\mathrm{d}V$ provides information regarding the orbital energies ξ_n. An independent way to extract ξ_n is by measuring the peaks in

the zero-bias conductivity versus gate voltage.

Within the scope of a non-interacting electron model these two methods should give the same results, but, as we will discuss later, taking into account electron-electron interaction makes the single-particle eigenstates sensitive to occupation numbers of other energy levels.

3.3. Experiments with Metallic Nanoclusters: Review

Metallic nanoclusters are 3-dimensional objects, so to get energy level spacing in a cluster at least 1 meV one should work with grains less than 10 nm.

Indeed, for a sphere of radius R

$$\delta E \approx E_{\rm F}/N = E_{\rm F}/\left(\frac{4}{3}\pi R^3 n\right). \tag{13}$$

For example, for aluminium, the Fermi energy $E_{\rm F} = 11.7$ eV, electron density $n = 18.1$ cm^{-3}, and $\delta E = 1$ meV for $R = 2.5$ nm.

Recently, two successful ways have been used to select one grain and to place it in a single electron transistor geometry. In one approach, tunneling contact with a particular grain was achieved in a 'vertical' geometry with a hole in silicon nitride membrane, where top and bottom electrodes are by chance connected via a few nanometer metallic dot[32,33]. In experiments of McEuen et al.[34], instead, a lateral geometry was used. Closely spaced electrodes, prepared in advance, were covered with a number of nanoclusters. Due to the exponential nature of tunneling, a single grain, well placed between the electrodes, controlled the transport in the device.

Unfortunately, there is very little control of the sample geometry at these sizes and measurements in the experiments described above have been performed on selected samples demonstrating a 'proper behavior'. Different techniques of self-assembling, promising a better control of the sample properties, are currently under development[35–37].

Fig. 16, reproduced from Ref. [33], shows a set of $I(V)$ curves for SET transistors building upon Al clusters with estimated radii of 4.5, 4.3, and 1.5 nm, respectively, for Figs. 16b-16d.

A set of corresponding ${\rm d}I/{\rm d}V$ curves is presented in Fig. 17. The ability to tune the number of electrons in a particle using V_g allowed, for the first time, to study the dramatic differences between tunneling spectra for even and odd numbers of electrons in the same superconducting particle.

Energy level spectra, extracted from ${\rm d}I/{\rm d}V$ measurements for different electron parities are presented in Fig. 18 as a function of magnetic field B.

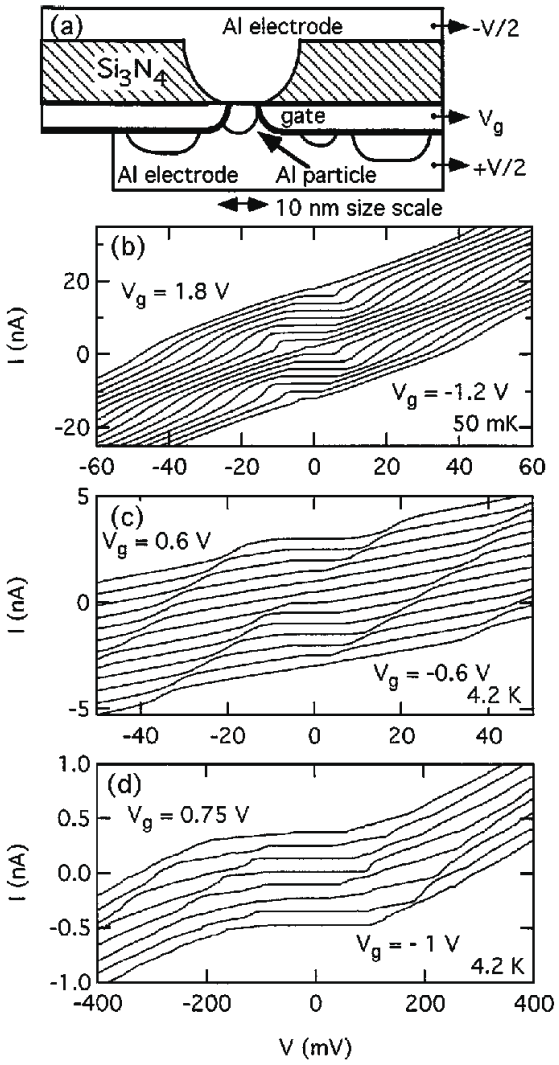

Fig. 16. **a.**-Schematic cross section of device geometry. **b.-d.**-Current-voltage curves displaying Coulomb-staircase structure for three different samples, at equally spaced values of gate voltage. Data for different V_g are artificially offset on the current axis. (From Ralph *et al.* [33].)

These data show how a magnetic field destroys superconductivity in a nanoparticle. Consider the second level at small B in Fig. 18a, which begins near 0.8 meV. This state shifts down as a function of B, due to

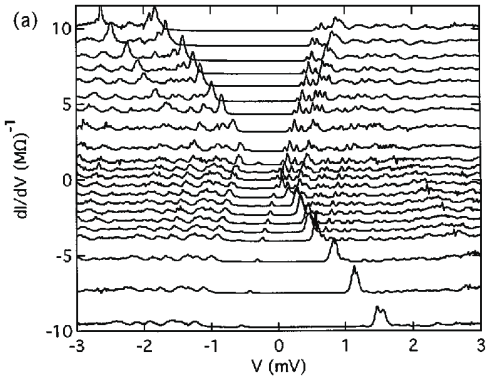

Fig. 17. dI/dV vs source-drain voltage, plotted for V_g ranging from 75 mV (bottom) to 205 mV (top), for the device of Fig. 16. Curves are offset on the dI/dV axis. (From Ralph *et al.* [33].)

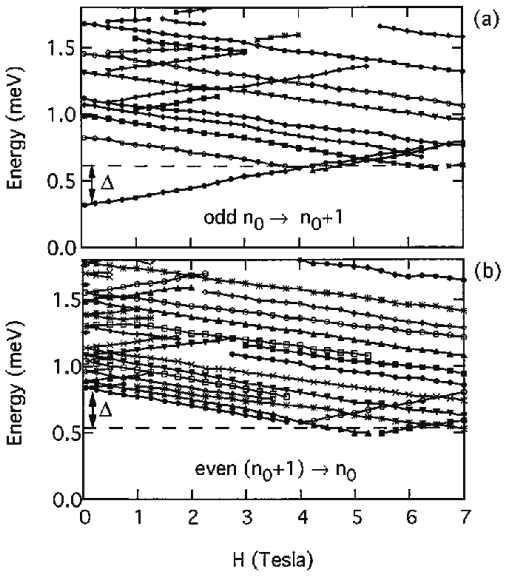

Fig. 18. Magnetic field dependence of the resolved electronic levels for the device of Fig. 16 at **a.**- $V_g \approx 110$ mV and **b.**- $V_g \approx 180$ mV. The dashed lines show the average energy of the tunneling threshold at large B. Superconducting gap $\Delta \approx 0.3$ meV. (From Ralph *et al.* [33].)

its spin-$\frac{1}{2}$ Zeeman energy, up to 4 T. There it disappears in favor of a new upward-moving (opposite spin-$\frac{1}{2}$) level. This means that the originally empty downward-trending level drops below the energy of an originally filled upward-trending level, and an electron is transferred between the states. The odd-electron ground state changes its spin from $\frac{1}{2}$ to $\frac{3}{2}\hbar$. As this process is repeated, the tunneling threshold moves in a continuous zigzag pattern, and the ground state successively increases its spin in units of $\hbar$. A similar argument for Fig. 18b shows that the even-electron ground state also evolves by individual spin flips. Superconductivity is destroyed as electrons flip one at a time. In contrast, the classic theories of Clogston and Chandrasekhar[38], for a superconducting transition driven by spin pair breaking, predict a large discontinuous jump in the tunneling threshold, at a field where many spins flip simultaneously. It's not clear yet whether these theories do not properly take into account the effect of discrete electronic energy levels in the particle, or whether the transitions are made continuous by some orbital pair breaking[39].

4. SPECTROSCOPIC MEASUREMENTS ON QUENCH-CONDENSED BISMUTH CLUSTERS

4.1. A Regular SET with 93 meV Charging Energy

Your sample is undefined.
Theoretician ⋆.

The tunneling spectroscopy measurements require a perfect SET transistor geometry. It was not obvious that such a clean geometry could be achieved by a rather simple technique involving random growth of a granular film. Our experiments show that the sample evolution *always* lead to a transistor with a regular gate dependence. A representative result of such an evolution is shown in Fig. 19.

A fit to the orthodox model gives a charging energy for this transistor of 93 meV (fit parameters: $C_1 = 2.3 \times 10^{-19}$ F; $C_2 = 4.6 \times 10^{-19}$ F; $C_{Gate} = 1.7 \times 10^{-19}$ F; $C_\Sigma = 8.6 \times 10^{-19}$ F).

To the best of our knowledge, this is the largest charging energy ever reported[10]. A well-formed diamond structure can be seen, with pronounced Coulomb staircases (marked with $\alpha_i \alpha_i'$ lines), and transistor is periodically open around zero bias with a gate voltage. The absence of Coulomb staircases parallel to the diamond edge γ indicates that the transistor is strongly asymmetric, with one tunneling resistance much greater than the other.

Besides the periodic staircase pattern in Fig. 19c some additional structures are also present. One can see a set of bright lines, reflecting enhanced differential conductance of the sample (one is marked by a line β). At low biases these lines tend to align parallel to each other, though their common angle β is different from the angles formed by the main Coulomb diamonds. As the bias is increased, these lines stick to the Coulomb steps. They are quasiperiodic with the main period of the transistor and tend to aggregate into clusters within one period. The principal question is: could they be attributed to a presence of some other islands nearby or do they reflect intrinsic spectral properties of the central island of a SET transistor?

The regular gate modulation in Fig. 19 is in contrast to all reported properties of single-electron devices based on random lateral structures, with reproducible, but irregular pattern of the current modulation by the electrostatic gate[41–43]. The presence of just one additional slope in Fig. 19 indicates that there are maximum two islands in a system (a three-island system will have at least three distinct slopes in the $\mathrm{d}I/\mathrm{d}V(V, V_g)$ pattern - see section 4.2. on page 35). The general case of two grains connected in series

[10] Transistor with charging energy $E_C = 55$ meV was reported in Ref. [40]. A device with $E_C = 115$ meV was mentioned, but no data were presented.

was considered theoretically by Rusin *et al.* in Ref. [44]. The stochastic nature of Coulomb blockade was predicted in the zero bias limit, and confirmed experimentally in Ref. [45]. Regular conductance oscillations at high temperatures transform into random peaks as the temperature is lowered, and finally, at zero temperature, the double-grain system is never opened, in contrast to our data in Fig. 19.

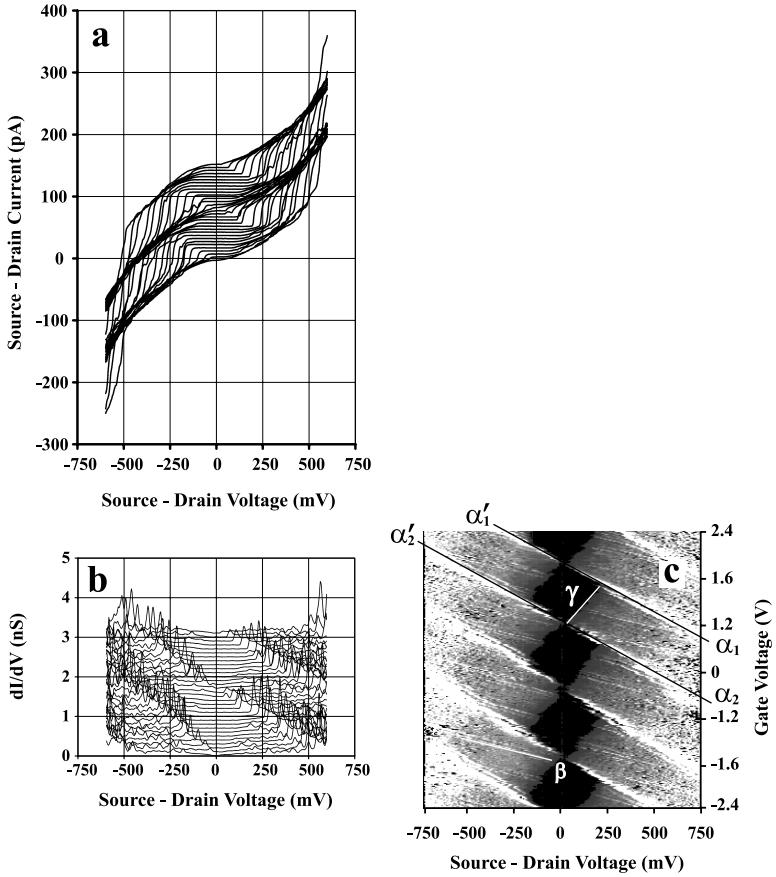

Fig. 19. A sample with regular gate dependency: **a.**- A set of $I(V)$ curves for different gate voltages shifted vertically for clarity. **b.**- A set of corresponding $\mathrm{d}I/\mathrm{d}V$ curves plotted for two gate periods (also artificially offset). **c.**- A gray-scale plot of $\mathrm{d}I/\mathrm{d}V(V, V_g)$ traced along five gate periods.

However, one can imagine a double-grain system of two non-equivalent grains. The first grain, the main one, forms an almost regular SET transistor, and the second one gives just a small perturbation, not disturbing an

orthodox diamond structure too much. To figure out what kind of perturbation we can expect from the second grain we have undertaken a systematic study of a double-grain system.

4.2. A Double-Grain SET

With twelve parameters one can fit anything!
Theoretician $\star\star$.

The current in a double-grain system could not be found analytically. So we made Monte-Carlo simulations using a commercial single electron circuit simulation software - SIMON 2.0[11]. Generally speaking, in a double-grain system we have five resistances and seven capacitances to play with (see Fig. 1 in Apeendix A) and a countless number of possible combinations. But for our samples (constrictions in granular films) we can assume that the tunneling gaps between grains are randomly and uniformly distributed from 1 Å to 10 Å. As a result, the tunneling resistances will be uniformly distributed in *logarithmic* scale from 10 KΩ and up to 100 GΩ. In fact, all observed samples with a well-formed periodic diamond structure were strongly asymmetric, with the only set of Coulomb staircases.

This circumstance reduces a continuum of possibilities to a very limited number of distinct topologies shown in Fig. 20. Indeed, the main tunneling gap (marked by a symbol R) can be placed between the lead and the smallest grain, like in Fig. 20a, or between two grains like in Figs. 20bc, or between the biggest grain and the lead. The latest case, not shown in Fig. 20, is trivial, as it reduces to a big gate-sensitive resistance, connected in series with a SET transistor[12]. The medium tunneling gap $\mathbf{R}$ and the smallest one $\mathbf{r}$ can then be placed in left-to-right or in right-to-left order. The resulting pattern, shown in Fig. 20a is essentially the same in both cases (only the relative intensity of the main staircases marked by $\alpha_i\alpha_i'$ and additional peculiarities marked by β_i is affected, provided $\mathbf{R} \ll \mathrm{R}$). The same is valid for configuration with the main tunneling gap separating two grains: Fig. 20b and Fig. 20c are topologically identical, and presented both just for comparison.

To summarise, for a system of two grains connected in series with one tunneling resistance much greater than the others, there are just three distinct topologies, determined by the location of the widest tunneling gap:

[11] URL: http://home1.gte.net/kittypaw/simon.htm

[12] As a result, the overall current modulation comes from the large grain, and a small staircases on $I(V)$ curves from the small one. This case was observed and dicussed in appended papers ## 1,2.

- between the smallest grain and the lead;
- between two grains;
- between the biggest grain and the lead (equivalent to a SET connected in series with a big gate-sensitive resistance).

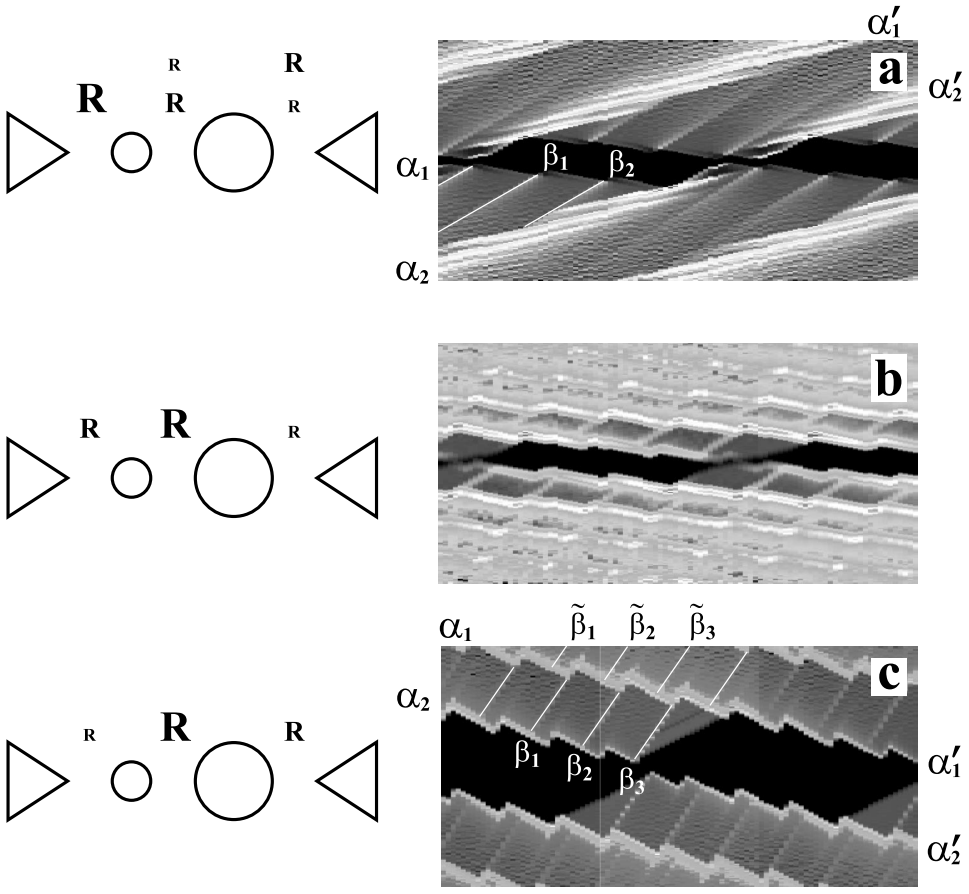

Fig. 20. A Monte-Carlo simulation result for a system of two grains connected in series: **a.**- The main gap between the small grain and the lead. **b,c.**- The main gap between two grains. α-lines mark coulomb staircases coming from the main tunneling gap, and β-lines - from the second one.

In both non-trivial configurations, additional perturbations β_i coming from the presence of a second grain are

- rectilinear,
- parallel to each other,
- equidistant,

unless the charge of the main grain remains constant (i. e. within an area confined by two near main staircases, for example, $\alpha_1\alpha_1'$-$\alpha_2\alpha_2'$). On crossing the primary staircase $\alpha_i\alpha_i'$ the whole family of secondary staircases β_i is shifted along the direction of α_i - compare β_i and $\widetilde{\beta_i}$ in Fig. 20c.

On the other hand, charge quantization in the small grain makes the main staircases α_i rippled.

There is one more nontrivial topology, when the second grain is placed outside the transport chain and affects the main transistor just electrostatically. This SET+SEB (Single Electron Box) hybrid topology is shown in Fig. 21. In fact, this is the most common source of sample imperfectness in our experimental situation. The tunneling conductance is a short-range phenomenon, while a capacitive coupling has a long-range effect, so it's more difficult to coalesce these electron boxes nearby by additional depositions than to reduce a transport chain to a single grain.

The second grain in this topology partially screens the gate potential influencing the main grain. Due to charge quantization in the single electron box this screening is non-continuos, and the effective gate potential, applied to the main grain, is stepwise modulated.

A simple transformation, demonstrated in Fig. 21b, allows to recover the diamond structure of the main transistor. The fragment of the $\mathrm{d}I/\mathrm{d}V$ pattern, confined by β_0-β_1, must be shifted by vector $\vec{\mathrm{V}}$, the fragment confined by β_{-1}-β_0 by vector $2\vec{\mathrm{V}}$, etc. Then we have to shift β_1-β_2 by $-\vec{\mathrm{V}}$, β_2-β_3 by $-2\vec{\mathrm{V}}$, and so on. An original diamond structure of the main transistor, restored as a result of this procedure, is shown in Fig. 21c.

This simulation was done for the main grain with a gap in the energy density of states slightly above the Fermy energy, to evaluate the effect of the second grain on tunneling spectroscopy data. This gap produces a dip in the $\mathrm{d}I/\mathrm{d}V$ pattern - a rippled dark line marked by γ in Fig. 21a. An analogous feature is also visible in Fig. 20c. We will discuss the possible influence of the second grain on spectroscopy data in section 5.4.

Although all assertions in this section were initially derived from numerous Monte-Carlo simulations, they were later confirmed analytically. A detailed theory can be found in Appendix A, we will just list the main results here.

- All Coulomb peculiarities in a double grain SET form straight lines in $\frac{\mathrm{d}I}{\mathrm{d}V}(V, V_g)$ plots.

- Each tunneling gap defines a set of peculiarities which are parallel to each other, so a double dot system has maximum five distinct slopes in the $\frac{\mathrm{d}I}{\mathrm{d}V}$ pattern. In a strongly asymmetric system, two staircase sets are suppressed, and only three distinct slopes survive.

- There could be maximum two grains in a system with three distinct staircase slopes.

- Although there is no more periodicity with respect to a gate voltage as in a single-dot system, the whole $\frac{\mathrm{d}I}{\mathrm{d}V}$ pattern is quasiperiodic. All staircases coming from the first grain have offsets proportional to $n_1 + (C/C_{\Sigma 2})n_2$, from the second one - $(C/C_{\Sigma 1})n_1 + n_2$, and from intergrain tunneling - $(C_{\Sigma 2} - C)n_1 - (C_{\Sigma 1} - C)n_2$, where $C_{\Sigma 1}$ and $C_{\Sigma 2}$ are the total capacitances of the first and the second grain respectively, and C is the inter-grain capacitance.

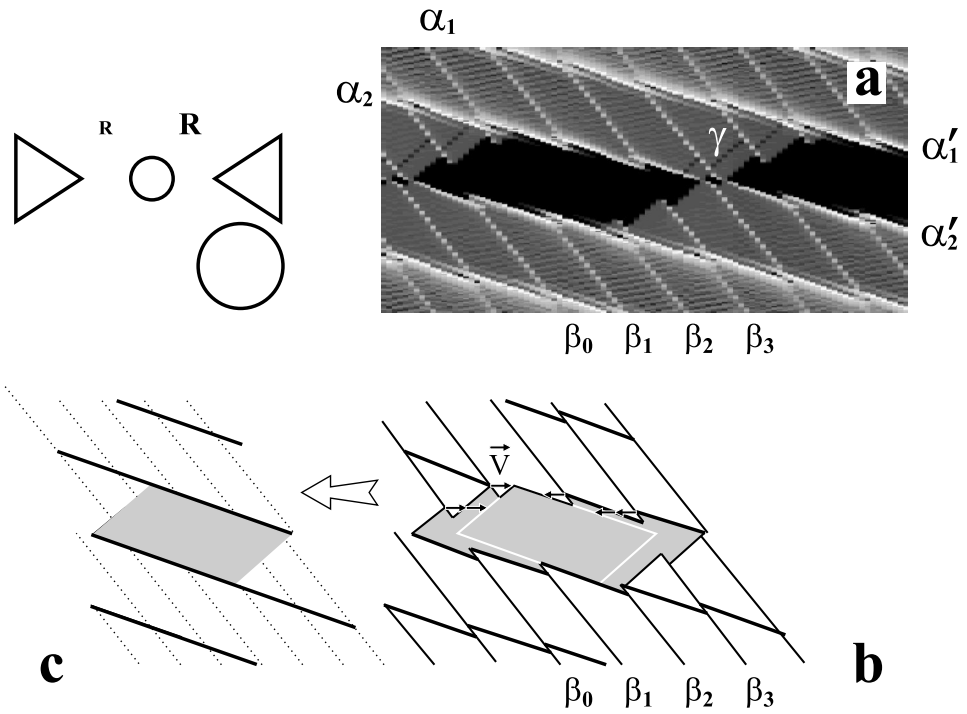

Fig. 21. SET+SEB hybrid topology: **a.**- The result of Monte-Carlo simulation. **b.**- The transformation procedure. **c.**- Recovered diamond structure of the main transistor. Secondary staircases are shown by dotted lines for reference only, they will be eliminated by this transformation.

- At any point (V, V_g) the intensity of a staircase line with an offset defined by some (n_1, n_2) combination depends on the probability $P_{n_1,n_2}(V, V_g)$ for a system to have n_1 electrons on the first grain and n_2 on the second. In a system with low charge fluctuations (an asymmetric case) n_1 is fixed within any area confined by two near primary staircases, and so all pecularities coming from the second grain are equidistant[13].

To summarise, for a system of two coupled grains the position of all peculiarities on $\mathrm{d}I/\mathrm{d}V(V, V_g)$ plot can be found analytically. The result of calculations shows that within the regions of a constant charge on the first grain (constricted by the main staircases in Fig. 19c) all peculiarities coming from the second grain are *straight* lines (in contrast to Fig. 19c, where they are curved when approaching the staircase), *parallel* to each other (this is the case), and exactly *equidistant* (in Fig. 19c they are obviously aggregated into clusters). Thus all attempts to explain the spectroscopic data from Fig. 19c by the presence of additional grains fail.

4.3. Tunneling Spectra of High-Ohmic Samples

One should not measure samples with resistance more than 1 GΩ.
August Yurgens.

High-ohmic samples with resistances exceeding a few GΩ demonstrated even more remarkable spectral features. A representative example is shown in Fig. 22. The sample in Fig. 22a was an immediate ancestor of that in Fig. 22c, i.e. they differ by a single deposition of just 1 Å of bismuth. Note that such a small amount of deposited material did not change the sample capacitances noticeably, but the sample resistance dropped forty times.

This is not surprising actually, as the tunnelling resistance is exponentially sensitive to the barrier width δ, whereas the grain capacitance is inversely proportional to the grain size R, provided δ is not much smaller than R. This is the case, as the sample radius, estimated from a fit to the orthodox model, is $R \approx 1.3$ nm, and 20 GΩ sample resistance implies the tunneling gap with $\delta \gtrsim 1$ nm (assuming tunneling through a vacuum)[14].

[13] For example, a spectral line marked with β_3 in Fig. 21c corresponds to a configuration $(n_1 = 0, n_2 = 0)$. When this line crosses the primary staircase $\alpha_1\alpha_1'$ it almost disappears, because the most probable charge configuration becomes $(-1, 0)$, and the probability of (0,0) fluctuation is almost zero.

[14] It's worth to mention here, that for high-ohmic samples the resistance changed stepwise during deposition, so any new-coming atom adsorbed by the grain or by the lead in the

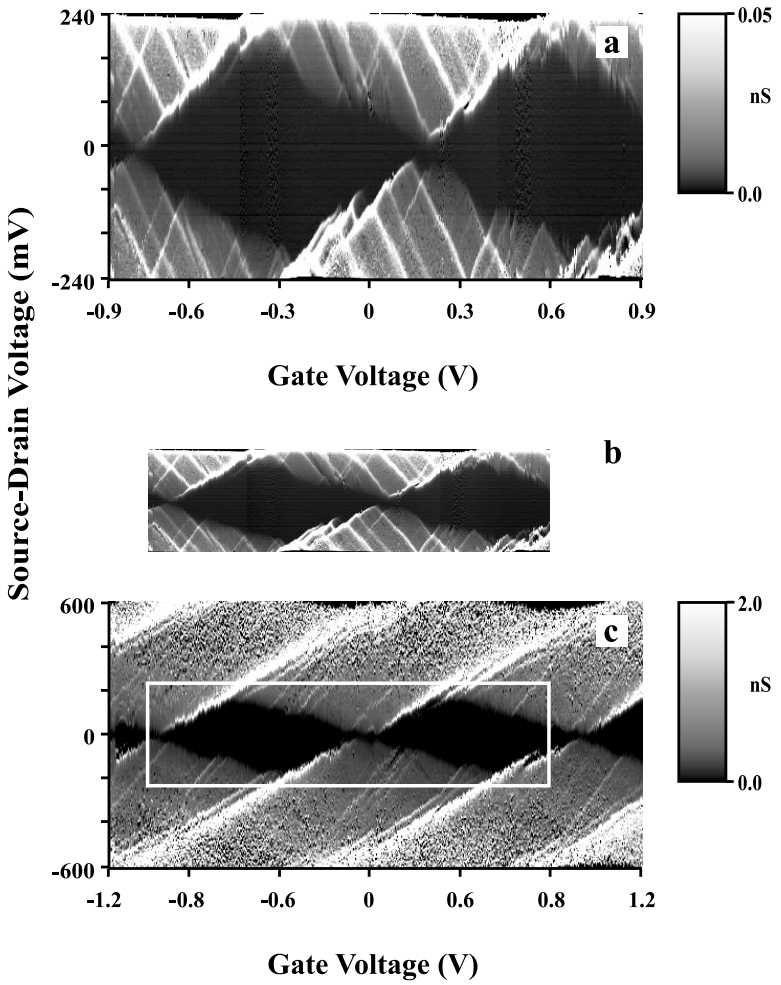

Fig. 22. Tunneling spectroscopy in a SET geometry: **a.**- Sample with the nominal film thickness 13.5 Å and 20 GΩ resistance. **b.**- Same as **a** but presented in the same scale as **c**. **c.**- The result of additional deposition of 1 Å. The white rectangle marks an area where data presented in **b** where taken. The sample resistance has dropped down to 0.5 GΩ, but the shape of the diamonds did not change.

Besides the main Coulomb staircases, well visible in Fig. 22, one can see some additional spectral lines. They are not equidistant within an area

vicinity of the contact, affected the gap width and the sample resistance. Statistically, the majority of new deposited atoms are adsorbed by the leads, and only those adsorbed by the grain itself will influence the grain radius.

confined by two nearly staircases, so they could not be attributed to a presence of a second grain in the system (and one can not assume more than one additional grain, because all additional lines have the same slope) - see section 4.2.

As it was explained in section 3.1., on page 20, if the central island of a SET transistor has any peculiarities in the energy density of states, additional lines will appear on $\mathrm{d}I/\mathrm{d}V(V, V_g)$ plot. If the energy spectrum in the grain does not depend on gate voltage, or, more generally speaking, on electrostatic field, then spectral lines will be parallel to each other and to the diamond edge. In contrast, our experimental data in Fig. 22 show a distinct slope for spectrum lines. The simplest interpretation is: in an extremely small grain the energy spectrum is sensitive to an electrostatic perturbation.

4.4. Screening in Metallic Nanoparticles

An external electrostatic field is screened within a thin (~ 1 Å) surface layer in a macroscopic metallic sample. From the macroscopic point of view, the electron concentration is slightly modified near the surface. Speaking the microscopic language, some electron levels with wave functions localised near the surface drop down in energy below E_F and become occupied[15]. The majority of electrons with energies close to the Fermi energy E_F are delocalised over the whole sample volume, and their wave functions do not overlap with a screened field. The scenario is different in a microscopic sample. An extreme microscopic case is an atom: an external electrostatic field modifies wave functions, but does not affect occupation numbers. This is because for an atom the typical energy level spacing δ is much greater than the level shift by an external field, and so the external field does not change occupation numbers. As a result, there is no screening in the atom, and all energy levels are sensitive to an electrostatic perturbation.

For our system we can assume some analogy with a jellium model for free metallic clusters[16]. In this model electrons with energies close to E_F are those with large orbital momentum numbers l and their wave functions tend to be localised near the cluster surface, and they are most sensitive to an external field.

Moreover, if we start from an assumption that there is no screening in our cluster, then we can roughly estimate the upper limit for a relative

[15] This is the starting point of a Thomas-Fermi approximation, which works well for a bulk metal: wave functions in a system do not change, the effect of an external field is a redistribution of occupation numbers - see Ref. [14], Chap. 17, pp. 344-348.

[16] We will discuss the applicability of a jellium model for our samples later in section 6.

energy level shift[17] by an electrostatic field $\mathcal{E}$ as $\delta E \sim e\mathcal{E}R$, where R is a cluster radius ≈ 1.3 nm, and $\mathcal{E} = V/L$, where V is a source-drain voltage ~ 100 mV and L is the lead-to-lead spacing $(3-5)$ nm. This gives us $\delta E \sim 30$ meV. For a cluster with 2000 valence electrons (see appended paper #4) we can estimate an energy level spacing $\approx \frac{2}{3}E_{\rm F}/N \sim 3$ meV. So only about ten electrons can change their occupation numbers. One can not treat the conducting electrons as a continuos fluid anymore and the macroscopic screening mechanism fails.

How will the ordinary spectroscopic picture, like the one sketched in Fig. 11, be modified for an extremely small sample with an energy spectrum sensitive to an external electrostatic field? To address this problem we have developed a program based on a direct numeric solution of the orthodox model. We will discuss the main numeric results in the next section.

4.5. Numeric Solution of Orthodox Model

Although there is no analytical expression for the current through a SET transistor, the orthodox theory[11,12] gives simple recurrent formulas expressing the probability $p_{n\pm1}$ for a dot to be charged with $n \pm 1$ electrons via p_n:

$$\begin{aligned} p_n &= p_{n-1}\frac{\overrightarrow{\Gamma}_1(n-1)+\overleftarrow{\Gamma}_2(n-1)}{\overleftarrow{\Gamma}_1(n)+\overrightarrow{\Gamma}_2(n)}, \quad \text{for positive } n, \\ p_n &= p_{n+1}\frac{\overleftarrow{\Gamma}_1(n+1)+\overrightarrow{\Gamma}_2(n+1)}{\overrightarrow{\Gamma}_1(n)+\overleftarrow{\Gamma}_2(n)}, \quad \text{for negative } n. \end{aligned} \tag{14}$$

Here $\overrightarrow{\Gamma}_i(n)$ and $\overleftarrow{\Gamma}_i(n)$ are the tunnling rates through gap i in left-to-right and right-to-left directions respectively. They can be found as

$$\overrightarrow{\Gamma}_{1,2} = \frac{\frac{1}{e}I_{1,2}\left(\frac{\Delta\overrightarrow{K}_{1,2}}{e}\right)}{1-\exp\left(-\frac{\Delta\overrightarrow{K}_{1,2}}{T}\right)},$$

[17] Note that for an electron with a wave function $|\psi_i\rangle$ an average value of the *absolute* energy level shift $\delta E_i = \langle\psi_i|eV|\psi_i\rangle$ is already taken into account by a capacitance model. What we have to estimate is a typical *relative* shift $\delta(E_i - E_j)$. Roughly speaking, we have to convolute the difference between two wave functions $|\psi_i\rangle$ and $|\psi_j\rangle$ and the external potential V. If, in an extreme case, $|\psi_i\rangle$ is localised, say, on the left side of the sample, and $|\psi_j\rangle$ on the right one, then $\delta(E_i - E_j) \sim e\mathcal{E}R$.

$$\overleftarrow{\Gamma}_{1,2} = \frac{\frac{1}{e} I_{1,2}\left(\frac{\Delta \overleftarrow{K}_{1,2}}{e}\right)}{1-\exp\left(-\frac{\Delta \overleftarrow{K}_{1,2}}{T}\right)}, \tag{15}$$

where $\Delta K_i(V, V_g)$ is the decrement in the electron's kinetic energy during the tunneling jump, and $I_i(V)$ is the current-voltage characteristics for gap i.

The programming implementation is rather straightforward: given recurrent equations for p_n, they can be immediately calculated, and one can find a current

$$I = \frac{e}{\Sigma} \sum_{-\infty}^{+\infty} \left(\overrightarrow{\Gamma}_1(n) - \overleftarrow{\Gamma}_1(n) \right) p_n, \tag{16}$$

where normalization factor Σ is given by the following sum:

$$\Sigma = \sum_{-\infty}^{+\infty} p_n.$$

The complete theoretical background and programming implementation details can be found in Appendix A.

To test the program we compared its output to the result of a Monte-Carlo simulation with SIMON. SET transistor parameters and the discrete energy levels for the central dot are shown in Fig. 23a. Note that each discrete level can only be occupied by a single electron (no spin degeneracy assumed). Left and right tunneling resistances were set equal.

As one can see, the program output, shown in Fig. 23c, is identical to MC simulations, presented in Fig. 23b[18].

A typical program execution time was below one minute (for an output $I(V, V_g)$ array of 256×256 points), whereas it took a few days to complete an MC simulation.

4.6. A Case of Central Grain with an Energy Spectrum Sensitive to an Electrostatic Field

In an asymmetric transistor with one dominating gap resistance, one set of spectral lines coming from the low-ohmic gap disappears, and only those features coming from the main tunneling gap survive. The numeric result for this situation is shown in Fig. 24a (compare it to a sketch in Fig. 11).

[18] One can qualitatively compare this plot to the measurement results in Fig. 15 on p. 26.

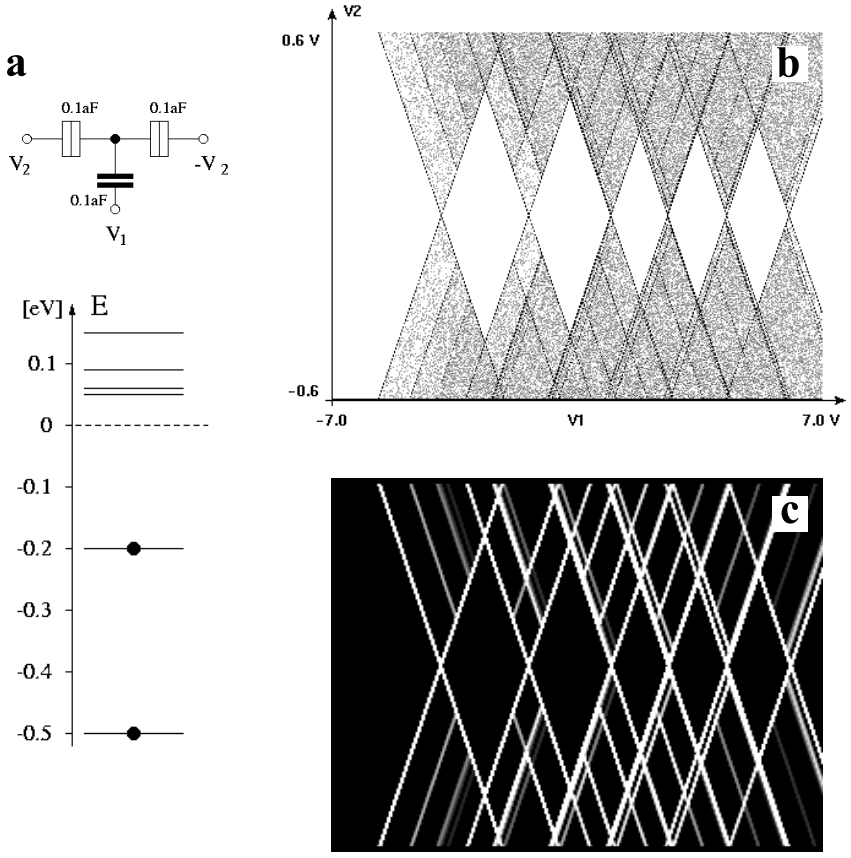

Fig. 23. Test run result: **a.**- An energy spectrum for central dot. **b.**- A stability plot simulated with MC method. **c.**- Program output. Note identical positions of spectral lines and equally sized diamonds. The relative intensity of spectral lines differs because of different brightness/contrast adjustment in **b** and **c**.

As it was explained in section 3.1. on page 21, in the asymmetric case a cross-section of an $I(V, V_g)$ plot along the direction of the main Coulomb staircases α gives essentially an $I(V)$ curve of the main tunneling gap. This $I(V)$ curve can be found as a convolution of two energy density of states, in the grain and in the lead. If the grain spectrum is quantized, then the convolution integral reduces to a sum:

$$I(V) = \frac{\delta}{e} G_1 \sum_k n_{\mathrm{F}}(\xi_k - eV)\Big[1 - n_{\mathrm{F}}(\xi_k - \mu_n)\Big], \tag{17}$$

where $n_{\mathrm{F}}(\xi)$ is a Fermi distribution function. At low temperatures ($T \ll \delta$)

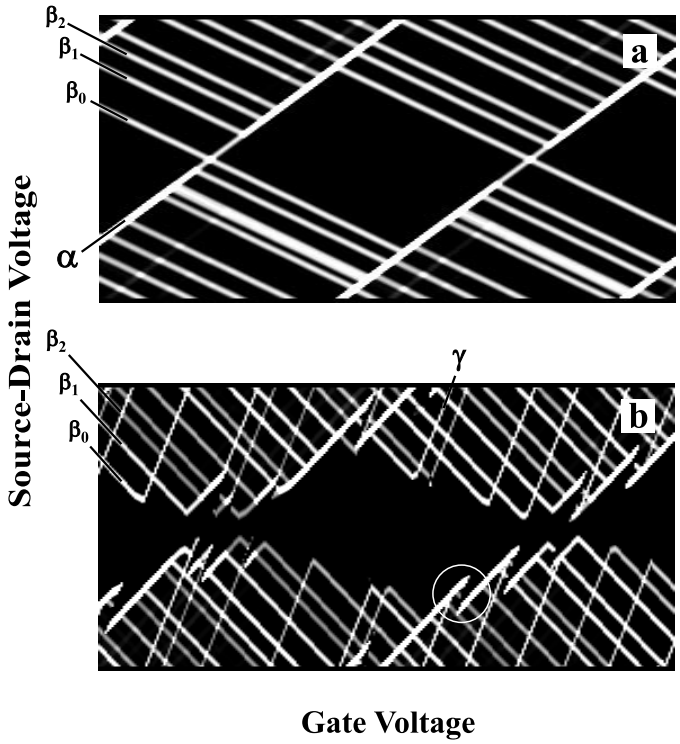

Fig. 24. Calculated $\mathrm{d}I/\mathrm{d}V$ plots for an asymmetric SET: **a.-** The energy spectrum of the central dot does not depend on external electrostatic fields. **b.-** All energy levels are shifted proportionally to some linear combination of V and V_g, but the chemical potential depends on the grain charge only.

System paremeters: $C_1 = 17 \times 10^{-20}$ F, $C_2 = 35 \times 10^{-20}$ F, $C_g = 23 \times 10^{-20}$ F, $R_1 = 1 \times 10^9$ Ω, $R_2 = 1 \times 10^7$ Ω.

the chemical potential μ_n in a grain charged with n electrons is:

$$\mu_n = \frac{\xi_{n+1} + \xi_n}{2}, \tag{18}$$

n numerates energy levels such that ξ_0 is the highest occupied state and ξ_1 is the lowest empty state in the *neutral* island. Formula (18) has a simple physical interpretation: at zero temperature all energy levels ξ_k with indexes $k < n$ (n is the number of additional electrons in a grain) are occupied, and the others are empty.

The tunneling $I(V)$ curve (17) has a step whenever eV exceeds the next energy level ξ_k, and these steps form spectral lines β_i in the $\mathrm{d}I/\mathrm{d}V(V, V_g)$ plot. If electrostatic fields do not influence the grain energy spectrum, then

all these lines are parallel to the line β_0 formed by the first step in the $I(V)$ curve, which marks the lowest unoccupied level, i.e. the position of the chemical potential in a grain, and forms the diamond edge.

If we simply assume now that the energy levels in a grain spectrum are uniformly shifted, say, with a gate potential V_g:

$$\xi_k(V_g) = \xi_k(0) + \alpha V_g, \tag{19}$$

substitute a modified $I(V)$ curve (17) into (15) then nothing interesting will happen with the spectroscopy pattern. The result of (19) reduces to a trivial renormalization of gate capacitance.

The data presented in Fig. 22a show a different behavior of spectral lines: they have a common angle different from the slope of the diamond edge, and the spectral lines *cross* the diamond edge. As the diamond edge is defined by the chemical potential, it may happen only if the energy levels are crossing the chemical potential in a grain.

So we shall assume the following model[19]:

$$\begin{aligned} \xi_k(V, V_g) &= \xi_k(0,0) + \alpha V + \beta V_g, \\ \textbf{and} \quad \mu_n(V, V_g) &= const. \end{aligned} \tag{20}$$

Surprisingly, such a simple modification of the orthodox model as (20), gives rise to a rich set of a new features in the $\mathrm{d}I/\mathrm{d}V$ pattern - see Fig. 24b:

- The spectral lines β_i start to cross the diamond edge, as it was expected.
- The main staircases become rippled.
- Within an area confined by two overlapping ripples (one is circled in Fig. 24) a region of negative differential resistance appears. A small satellite peak is splitted away from the main Coulomb staircase, and $\mathrm{d}I/\mathrm{d}V$ is negative in-between.
- The spectral lines β_i "reflect" from the diamond edge, and new lines with a slope γ appear.

All these features were observed experimentally in the $\mathrm{d}I/\mathrm{d}V$ plot of sample presented in Fig. 22a.

The most remarkable feature in Fig. 24b is a new set of spectral lines γ. Their formation mechanism, illustrated in Fig. 25, is completely different from an orthodox scenario.

[19] There is an internal contradiction in this model, which we will discuss in section 5.1., but first we would like to describe the consequences of (20).

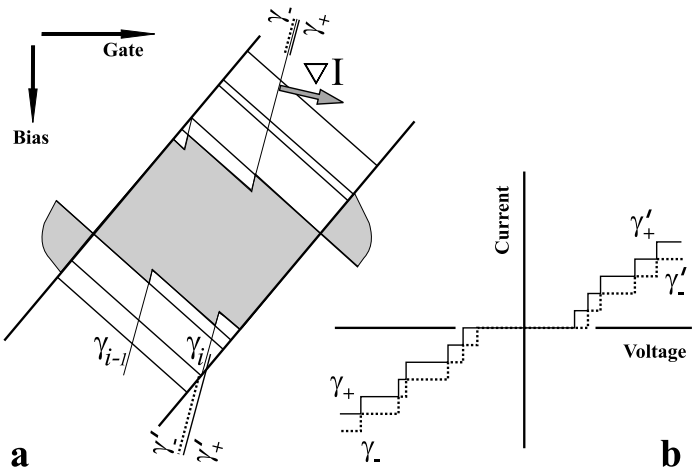

Fig. 25. Formation of new spectral lines in an $\frac{\mathrm{d}I}{\mathrm{d}V}(V, V_g)$ plot: **a.**- A spectral line γ_i separates two regions in the (V, V_g) plane: some energy level ξ_i is below the chemical potential on the left and above on the right. **b.**- Two cross-sections of an (not shown) $I(V, V_g)$ plot: solid line - $\gamma_+\gamma'_+$, taken slightly above γ_i; dotted line - $\gamma_-\gamma'_-$, taken below γ_i. Both curves have identical positions of current steps, but for the solid curve current exceeds its value for the dotted curve by one current increment.

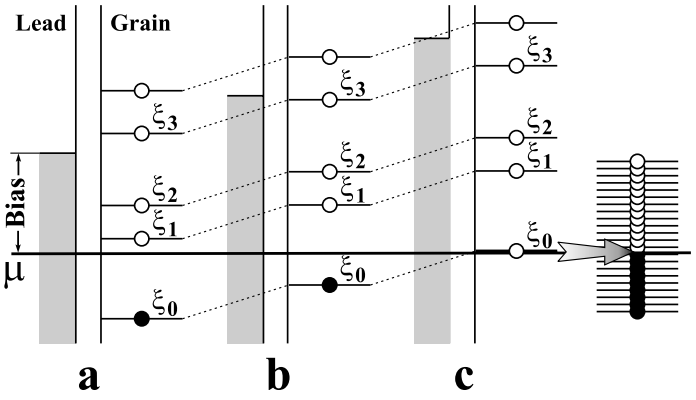

Fig. 26. Two different mechanisms for current steps: **a.**- Two energy levels, ξ_1 and ξ_2, are open for transport. **b.**- Bias exceeds ξ_3. One additional transport channel opens, resulting in a stepwise increment in current. **c.**- At some other bias ξ_0 exceeds the chemical potential μ. Occupation number at ξ_0 changes from 1 to 0. ξ_0 starts to contribute to the current.

For any energy level ξ_i in a grain spectrum, a corresponding γ_i-line is defined by the condition $\xi_i(V, V_g) = \mu$, i.e. the γ_i-line splits the (V, V_g) plane into two regions: $\xi_i(V, V_g) < \mu$ on the left side, and $\xi_i(V, V_g) > \mu$ on the right one. Whenever some energy level crosses a chemical potential, the whole $I(V)$ curve is incremented, as shown in Fig. 25b. So two cross-sections of $I(V, V_g)$ plot - $\gamma_+\gamma'_+$ slightly below γ_i, and $\gamma_+\gamma'_+$ above γ_i,- will give different $I(V)$ curves, shown in Fig. 25b by solid and dotted lines respectively. This results in a current step in the $I(V, V_g)$ plot, with a gradient in the direction indicated by vector $\bigtriangledown\mathbf{I}$ in Fig. 25a. A component of the gradient $\bigtriangledown\mathbf{I}$ along the V-axis gives a spike in the $\frac{\mathrm{d}I}{\mathrm{d}V}(V, V_g)$ plot - a spectral line γ_i.

A more qualitative explanation is illustrated in Fig. 26. When the main tunneling gap is biased, a current is incremented any time the bias exceeds the next energy level in a grain spectrum, as in Fig. 26b. These current increments result in orthodox spectral lines with slope β in Fig. 24. But the current is also incremented if some energy level is shifted by an electrostatic perturbation above the chemical potential. This mechanism, sketched in Fig. 26c, gives an additional set of spectral lines γ.

5. TWO-LIQUID MODEL

We will start this section by introducing the two-liquid model. Then we will discuss why some alternative suggestions, like the presence of a second grain (5.2.-5.4.), a non-equilibrium distribution of electrons in the grain (5.5.), or possible anomalies in the barrier transparency (5.6.) do not explain the experimental data. A physical justification of the two-liquid model will be discussed later in section 6.

5.1. Model Description

As illustrated in Fig. 26c, any time an energy level crosses the chemical potential, its occupation number changes from unity to zero. But the electron can not leave the grain, as the total number of electrons is fixed by Coulomb blockade, and, of course, it can not just disappear. There must be some other quantum states in the grain, not visible in the spectroscopy pattern. So we shall assume the following model, which we will refer later to as the two-liquid model:

There are two different electron communities in a grain:

- Electrons from the first group do not contribute noticeably into current transport, but they form the majority of quantum states in the grain and define the chemical potential.

- Electrons from the second group dominate the transport. Their energy levels are shifted by an electrostatic perturbation with respect to a chemical potential, fixed by electrons from the first group.

When an electron from group II leaves its energy state, it occupies some quantum state of type I, as shown in Fig. 26c. If we assume that the mean energy spacing between levels of type I is negligible, then the energy of the highest occupied state (the chemical potential) will not change. And as the electron is still inside the grain, the Coulomb energy of the system will not be affected either.

In the next sections we will discuss possible realizations of the two-liquid model.

5.2. A Double-Grain SET with T-shape Topology

A trivial idea, which actually does not work, as we will see later, is illustrated in Fig. 27. One can consider a double-grain SET with only one grain

coupled to the leads. So all current flows through the first grain only, which is small enough and has a discrete energy spectrum. The second grain is, say, two times bigger, and has an average energy level spacing ten times smaller, so we can assume a continuos spectrum for it. The inter-grain resistance should exceed $\hbar/e^2$ to keep the first grain spectrum quantized[20], but the capacitance coupling should be strong enough, so that an electrostatic energy increment during grain-to-grain tunneling is much smaller than e^2/C_Σ.

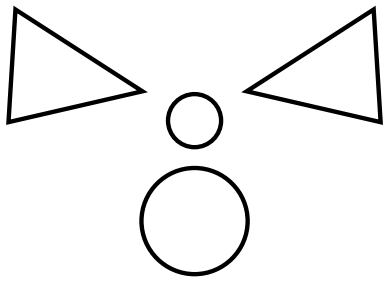

Fig. 27. A double-dot SET with T-shape topology.

To say it simple, we would like to build a system with some common charging energy, which, like a single dot, has a regular non-disrupted diamond structure, but actually consists of two grains. The smallest grain provides spectral lines in a dI/dV plot. The second grain does not participate in current transport and serves only as a reservoir to define a common chemical potential μ. If two grains have different gate (lead) capacitances, then the gate (source-drain) voltage will shift small grain spectrum with respect to μ.

To check this explanation, we have developed a program for a numeric solution of the orthodox model for a double-grain SET with arbitrary topology. We will briefly describe the numeric details in the next section. Then, in section 5.4. we will show that the numeric results for T-shape model show that this model cannot explain our experimental data.

5.3. Numeric analysis of a Double-Grain SET

There is no analytic solution for a double-dot SET. Even numerically, equilibrium probabilities $p_{n1,n2}$ for different charge configurations cannot

[20] As we will discuss in section 6.2., if an energy spectrum in the big grain has well-formed shell structure, then some regions of discrete spectrum still survive in the small grain even if $R \sim \hbar/e^2$.

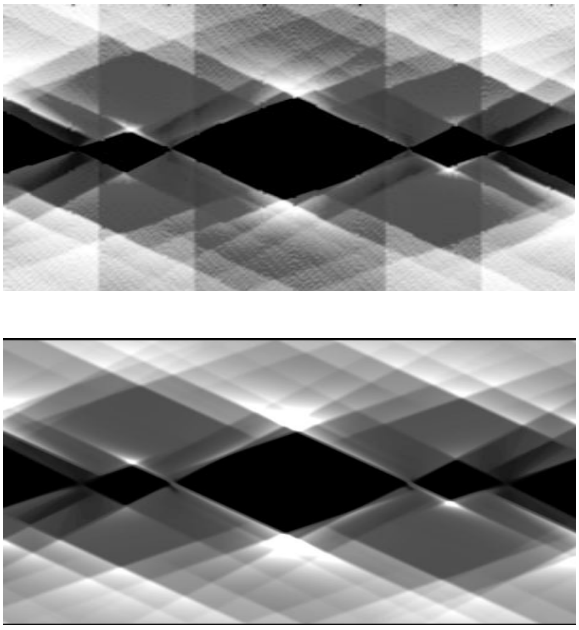

Fig. 28. General case of a double-dot SET: **a.**- The result of Monte-Carlo simulation. **b.**- Direct numeric integration of master equation.

System parameters: $C_{11} = 16 \times 10^{-20}$ F, $C_{12} = 8 \times 10^{-20}$ F, $C_{21} = 9 \times 10^{-20}$ F, $C_{22} = 13 \times 10^{-20}$ F, $C_{g1} = 8 \times 10^{-20}$ F, $C_{g2} = 11 \times 10^{-20}$ F, $C = 10 \times 10^{-20}$ F, $R_{11} = 3 \times 10^{9}$ Ω, $R_{12} = 2 \times 10^{9}$ Ω, $R_{21} = 1 \times 10^{9}$ Ω, $R_{22} = 2 \times 10^{9}$ Ω, $R = 20 \times 10^{9}$ Ω.

be calculated directly via recurrent formulas like (14). The only way is to integrate numerically a dynamic master equation for the evolution. The underlying formulas are too bulky to be presented here - one should look in Appendix A for details.

To test the program, we first simulated an arbitrary double-dot system with the Simon program, and then compared a Monte-Carlo simulation result with the program output - see Fig. 28. As one can see, all Coulomb peculiarities have identical positions in both Fig. 28a and Fig. 28b.

Both grains in the system presented in Fig. 28 have continuos spectra. An ultimate test would be to simulate a system with a discrete spectrum at least in one grain. Unfortunately, even for the system in Fig. 28a it took a few days to complete the MC simulation[21] (and a few minutes to calculate Fig. 28b[22]). In the case of a discrete spectrum an estimated MC simulation

[21] On a Sun SPARC-station.
[22] On a Pentium-pro PC.

time rises up to a few months.

5.4. Spectral Pattern for a Double-Grain SET with T-shape Topology

Fig. 29 shows the effect of a second grain on the spectral pattern in a T-shape topology. The first grain has the same capacitances as the one in Fig. 23, but asymmetric resistances to highlight peculiarities coming from one tunneling gap. The second grain has approximately three times greater capacitance and is connected resistively to the first grain, but not to the leads.

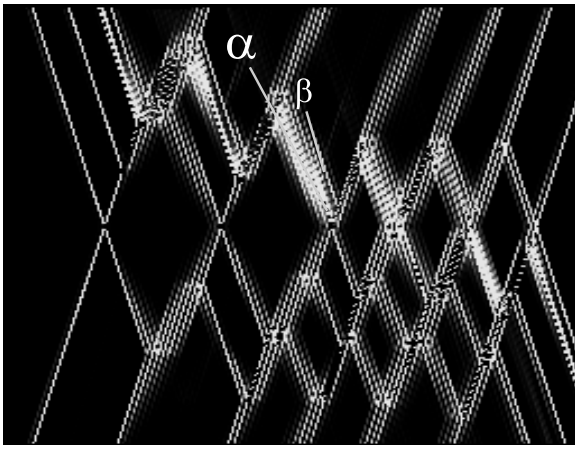

Fig. 29. The influence of a second grain on the spectral pattern in a T-shape topology. Original spectral lines with slope α are split into multiplets with slope β. β-lines intersect diamond edges. System parameters: $C_{11} = 10 \times 10^{-20}$ F, $C_{12} = 10 \times 10^{-20}$ F, $C_{21} = 29 \times 10^{-20}$ F, $C_{22} = 31 \times 10^{-20}$ F, $C_{g1} = 10 \times 10^{-20}$ F, $C_{g2} = 33 \times 10^{-20}$ F, $C = 12 \times 10^{-20}$ F, $R_{11} = 1 \times 10^{9}$ Ω, $R_{12} = 1 \times 10^{7}$ Ω, $R_{21} = 1 \times 10^{12}$ Ω, $R_{22} = 1 \times 10^{12}$ Ω, $R = 1 \times 10^{10}$ Ω.

The result presented in Fig. 29 is easy to understand. The charge q_2 on the second grain fluctuates, and for any given q_2 an effective energy spectrum of the first grain is shifted up or down in energy. As a result, any energy level in the original spectrum is split into a multiplet.

As the capacitance of the second grain is larger, it accumulates more electrons at a given gate voltage. So as the gate potential is increased, time by time some electron leaves the first grain and jumps into the second one.

At that moment, line β reaches the diamond edge. As expected, the diamond edge (the chemical potential) is defined by electrons in the biggest grain.

Varying system parameters, one can increase the β-line splitting, but not too much - it must be small in comparison with the size of the diamond. Otherwise the side-lines of a multiplet will be suppressed, as the probabilities of all but one charge configuration in multiplet will drop to zero. For the same reason, the length of the β-line in this model can never exceed the size of the diamond edge, in contrast to data presented in Fig. 22a. Moreover, no 'reflected' lines like γ-lines in Fig. 22a appear.

There is one more problem: we can estimate a typical inter-level spacing in a grain spectrum from the data in Fig. 22a as 30 meV. As we see, the presence of the second grain can only increase the number of peculiarities in the $\mathrm{d}I/\mathrm{d}V$ plot. To generate a pattern like Fig. 22a we have to assume an inter-level spacing in the original grain spectrum greater than $(100 - 150)$ meV, which is non-realistic.

To summarise, a T-shape model can not explain our experimental data.

5.5. The Effect of Non-Equilidrium Distribution Function

Formula (18) for the chemical potential μ is valid only for a grain in thermodynamic equilibrium at zero temperature. For the equilibrium distribution at finite temperature, μ is decremented by $\sim T^2$, i.e. the temperature shifts the chemical potential with respect to energy levels in a grain spectrum. Non-equilibrium effects in a grain are to some extent analogous to heating[23]. We can expect that an effective chemical potential μ^{eff} for non-equilibrium distribution function[24] will be shifted with respect to its value at equilibrium; the more the deviation from equilibrium, the greater the shift. Could the observed crossing of spectral lines and the diamond edge be explained by this effect?

To check this hypothesis we have developed a program for an extreme case when there is no relaxation in a grain. It means that if an electron jumps into a grain and occupies an energy level ξ_i, it will occupy ξ_i until it will jump out. And vice versa: if some electron jumps out and leaves a hole, the hole will not be occupied until some other electron will jump into this particular state[25].

[23] We cannot assume overheating in the leads - it will result in smearing the Coulomb staircases, and these are well pronounced in our experimental curves.

[24] We can define μ^{eff} for a non-equilibrium distribution by the condition that the total number of holes below μ^{eff} equals the total number of electrons above μ^{eff}.

[25] It should be pointed out here, that we assume a non-interacting electron model, i.e. an energy level ξ_i does not depend on the occupation numbers for other levels. Non-

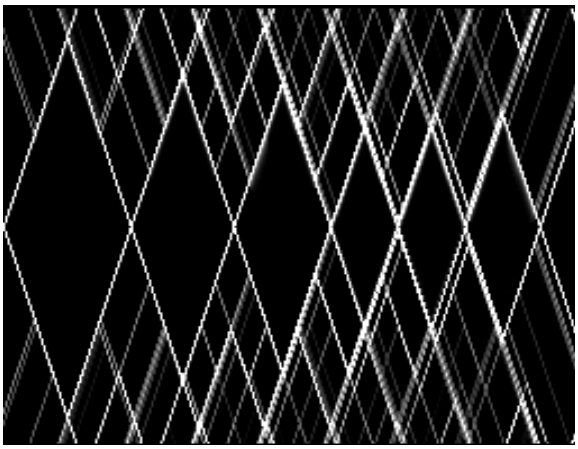

Fig. 30. The case of no thermal relaxation in a grain.

Program realization details are, as usual, presented in Appendix A. The result is shown in Fig. 30.

As one can see, turning off the relaxation in a grain has no dramatic effect on the spectroscopy pattern. Some additional spectral lines, not present in Fig. 23, appear, especially at higher biases. This is because some electron levels, always empty in equilibrium configuration, can now be occupied, contributing to tunneling rates $\overleftarrow{\Gamma}_1$ and $\overrightarrow{\Gamma}_2$, and some energy levels, always occupied at thermal equilibrium, can now be empty, contributing to $\overrightarrow{\Gamma}_1$ and $\overleftarrow{\Gamma}_2$. But spectral lines do not cross the diamond edges, and no new lines with a slope different from that of the diamond edges arise.

5.6. Anomalies in Barrier Transparency

In principle, tunneling barrier transparency as a function of energy may have resonance singularities. It may happen if the barrier potential has some quasi-bounded states. For example, there may be a stand-alone atom inside the barrier, a trap in the Al_2O_3 substrate, a charged defect etc. - too many opportunities to be listed. Any resonance in barrier transparency will give an additional spectral line in the $\mathrm{d}I/\mathrm{d}V$ plot.

This explanation is irrelevant to the presence of a small grain in a transport chain - the same mechanism should work for two macroscopic leads separated by a single tunneling gap. Depositing more material we can merge a central grain with one of the leads. In fact, all samples in our experiments

equilibrium effects for interacting electrons were considered in Refs. [46–48] and [13,49].

eventually evolved into this single gap topology. There was no gate dependency for single gap structures and no spectral features were ever observed in $\mathrm{d}I/\mathrm{d}V$ plots over the whole range of sample resistances 1 MΩ − 10 GΩ.

We can argue, therefore, that the barrier transparency for our samples is a regular function of energy, and all peculiarities on spectroscopy pattern come from the presence of the grain itself.

6. POSSIBLE PHYSICAL IMPLEMENTATIONS OF THE TWO-LIQUID MODEL

We will start this section with a short description of shell effects in free metallic clusters. As we will see, a small metallic cluster is not a piece of metal, just a small one. The Fermi energy in a small metallic cluster is usually placed within a gap in the density of states. This gap arises from a spontaneous reconstruction of the ground state accompanied by the formation of a shell structure in the energy spectrum. A typical gap value is a few hundred meV, so the bulk energy states are excluded from the low-bias tunneling transport. On the other hand, the gap in the energy spectrum implies the possibility of the existence of surface states, which dominate the low-bias transport.

6.1. Shell Effects in Finite Fermion Systems: Elementary Introduction

Quantization of a system of particles in a finite spatial domain leads to discrete energy eigenvalues, which are usually grouped into bunches of degenerate levels, called shells. The amount of bunching depends on the symmetry of the confining potential. For fermion systems obeying the Pauli principle, this leads to shell effects which are well-known in atoms and nuclei (see Ref. [16,17]): local minima in the total binding energy per particle versus particle number or deformation, sawtooth-like behavior of the particle separation energy (ionization potential, electron affinity). These effects can be described theoretically in terms of independent (or weakly interacting) fermions moving in a common potential. Inversly, the experimental observation of shell effects suggests the existence of a mean field in which fermions move more or less independently.

The occurrence of shells of single-particle levels is a global phenomenon in the sense that they depend more on the overall form of the mean field (e.g., symmetry, steepness of the surface, deformation) than on the finer local details of its radial dependence. This explains the great success of the so-called jellium model.

The basic idea of the self-consistent jellium model is to replace the distribution of ionic cores by a constant positive background or jellium density in a finite volume and to treat the valence electrons in the mean-field approximation.

As a first approximation, we can assume the jellium density to be spherically symmetric. Such a potential automatically gives rise to spherical shell structure because of its symmetry. Each shell is characterized by the ra-

dial quantum number n and the angular momentum l. For the electronic system with exactly the right number of electrons to complete a shell, the energy has a minimum with respect to small deviations from the spherical symmetry. When a spherical l shell is only partially filled, the system lifts the degeneracy of its ground state by allowing the mean field to give up spherical symmetry, resulting in an energy gain.

To find this spontaneous deformation, one varies the shape of the jellium density distribution and lets the electrons adjust themselves in the corresponding deformed ionic potential. The ground-state configuration is then found recursively by minimizing the total energy with respect to the jellium shape (practically, one parametrizes the shape of the jellium density in terms of one or several deformation variables).

The shells are not only peculiar to spherical systems, in fact, the mere existence of spontaneous deformation of the ground state (well known effect in the nuclear physics) is due to shell effects. What *is* crucial, however, is the flexibility of an ionic subsystem. If ions are stabilized (a metallic grain in an oxide matrix, for example) then there will be no shell peaks in the energy spectrum.

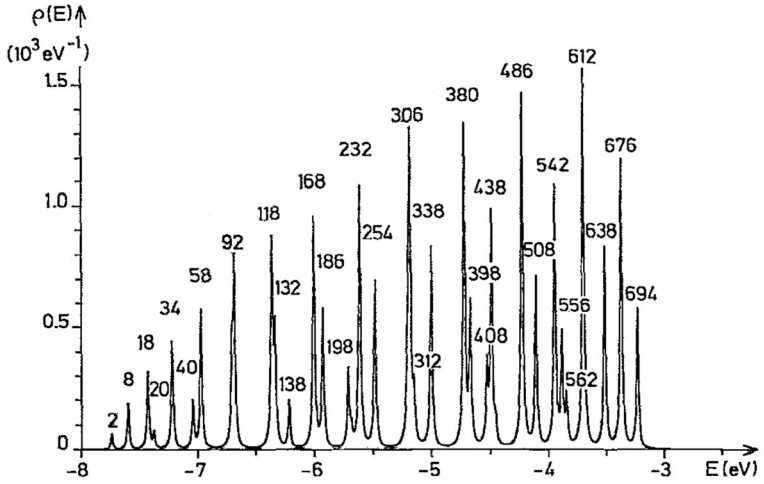

Fig. 31. Independent electron-state densities in a cluster of 704 lithium atoms, computed using the spherical jellium background model as solved self-consistently in the local-density approximation. The Wigner-Seitz radius is taken as $r_s = 2\mathring{A}$. (From Bréchignac *et al.* [50].)

Fig. 31, reproduced from Ref. [50], shows the electron-state densities

computed using the jellium model for a cluster with $N = 704$ electrons. Note that the Fermi level is placed within the gap between shells. This follows from the common variation principles: if the density of states (DOS) has a maximum at the Fermi energy, then, most likely, a small variation of the confining potential will shift the DOS peak position, thus minimizing the total energy.

6.2. Two Clusters with a Point Metallic Contact

As the next step we will consider a simple system: two grains bridged with a small (atomic-size) metallic link. A double-grain system with a tunneling link was considered in section 5.2. It was shown that it can not explain the $\mathrm{d}I/\mathrm{d}V$ pattern observed in our experiments. A metallic contact between two grains will normally lead to hybridisation of the wavefunctions in the two grains, so that any electron will be delocalised over both grains. As we will see below, the situation is very different, if we assume that the grain spectrum has a shell structure.

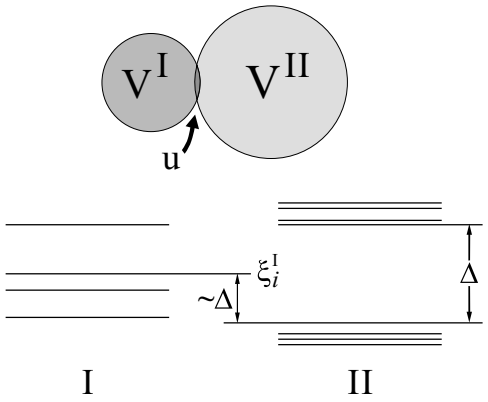

Fig. 32. A simple model for two clusters having an atomic size contact: two 3-d potential wells overlapping over a small volume u. The shell formation in cluster II leads to a gap Δ in the energy spectrum. The details of non-perturbed spectrum in a small grain are not important - the spectrum will be randomized due to coupling to a big grain.

Suppose we have two 3-dimensional potential wells, with potentials V^{I} and V^{II} (see Fig. 32). If V^{I} and V^{II} do not overlap, then we have two

independent Hamiltonians, and two sets of eigenfunctions:

$$\begin{aligned} H^{\rm I}\Psi_i^{\rm I} &= \left(\frac{1}{2m}P^2 + V^{\rm I}\right)\Psi_i^{\rm I} = \xi_i^{\rm I}\Psi_i^{\rm I}, \\ H^{\rm II}\Psi_j^{\rm II} &= \left(\frac{1}{2m}P^2 + V^{\rm II}\right)\Psi_j^{\rm II} = \xi_j^{\rm II}\Psi_j^{\rm II}. \end{aligned} \tag{21}$$

Now let $V^{\rm I}$ and $V^{\rm II}$ overlap over a small volume u. We would like to estimate the first nonvanishing corrections to $\Psi_i^{\rm I}$ and $\xi_i^{\rm I}$. Following the standard perturbation technique, we search for a solution of the common Hamiltonian[26]

$$\left(\frac{1}{2m}P^2 + V^{\rm I} + V^{\rm II}\right)\widetilde{\Psi}_i^{\rm I} = \widetilde{\xi}_i^{\rm I}\widetilde{\Psi}_i^{\rm I} \tag{22}$$

in a form

$$\widetilde{\Psi}_i^{\rm I} = \Psi_i^{\rm I} + \sum_j C_j\Psi_j^{\rm II} + \sum_{k\neq i} D_k\Psi_k^{\rm I}. \tag{23}$$

Substituting (23) into (22) and keeping the leading terms only, we have:

$$\widetilde{\Psi}_i^{\rm I} = \Psi_i^{\rm I} + \sum_j \frac{\langle\Psi_j^{\rm II}|V^{\rm II}|\Psi_i^{\rm I}\rangle}{\xi_i^{\rm I} - \xi_j^{\rm II}}\Psi_j^{\rm II}, \tag{24}$$

and

$$\widetilde{\xi}_i^{\rm I} = \xi_i^{\rm I} + \langle\Psi_i^{\rm I}|V^{\rm II}|\Psi_i^{\rm I}\rangle. \tag{25}$$

The term with the sum over $\Psi_k^{\rm I}$ in (23) is not important for the future and is omitted in (24).

If we assume that $V^{\rm II}$ is smooth (this is the case for the jellium model) we can roughly estimate the matrix element in (24) in the case if the overlapping volume u is about one elementary cell as

$$\langle\Psi^{\rm II}|V^{\rm II}|\Psi^{\rm I}\rangle \sim E_{\rm F}\frac{1}{\sqrt{\rm V_1}}\frac{1}{\sqrt{\rm V_2}}u = \frac{E_{\rm F}}{\sqrt{N_1N_2}}, \tag{26}$$

where $\rm V_1$ and $\rm V_2$ are cluster volumes, $E_{\rm F}$ is the Fermi energy and N_1 and N_2 are the number of atoms in the first and the second clusters respectively.

If the energy spectrum for $H^{\rm II}$ has a gap Δ, and $\xi_i^{\rm I}$ is within this gap, then the denominator in (24) never goes to zero, and the perturbation procedure is correct. If $\xi_i^{\rm I}$ is at some energy $\xi \sim \Delta$ above the gap bottom, then the main contribution in (23) comes from $\approx \frac{\Delta}{\delta_2}$ energy levels close to the energy gap (δ_2 is an average interlevel spacing in the second cluster), with

$$C_j \approx \frac{E_{\rm F}}{\Delta}\frac{1}{\sqrt{N_1N_2}}. \tag{27}$$

[26] We assume that $V^{\rm II}\Psi^{\rm I}$ and $V^{\rm I}\Psi^{\rm II}$ are vanishingly small everywhere except in u.

So we can evaluate the probability for an electron in state $\Psi_i^{\rm I}$ to be found in the second cluster as

$$P = \sum_j |C_j|^2 \sim \frac{\Delta}{\delta_2} \times \left(\frac{E_{\rm F}}{\Delta} \frac{1}{\sqrt{N_1 N_2}} \right)^2 = \frac{\delta_1}{\Delta}, \tag{28}$$

(we assume that the average interlevel spacing in the first cluster $\delta_1 \sim E_{\rm F}/N_1$ and in the second one $\delta_2 \sim E_{\rm F}/N_2$).

Note, also, that (25) gives for the energy shift

$$\sim E_{\rm F}/N_1 = \delta_1 < \Delta. \tag{29}$$

There is a simple classical interpretation of formula (29):

An electron with speed $v_{\rm F}$ passes $v_{\rm F}/a$ elementary cells per unit time (a being a lattice parameter). So the probability to visit particular cell per unit time is $v_{\rm F}/(aN)$, where N is the number of atoms in a cluster, or in energy units

$$\frac{\hbar v_{\rm F}}{aN} \sim E_{\rm F}/N. \tag{30}$$

For clusters connected via an atomic-size metallic contact we can assume a simple model: if an electron hits the cell which bridges two clusters, it jumps through with the probability 100%. Then (30) is a good estimate of the electron's escape rate, or, in energy units, the hopping integral.

To summarize, even if two clusters have a metallic contact (atomic-size), but there is a gap in the second cluster's spectrum, then all electrons in the first cluster with energies within this gap are still localized in the first cluster.

As one can see in Fig. 31, the highest energy shell peak for a lithium cluster with 700 electrons is $\frac{1}{2}\Delta \approx 300$ meV below $E_{\rm F}$. As Δ roughly scales proportionally to $E_{\rm F}$ and inversely proportionally to $\sqrt{N}$, an expected value for a bismuth cluster with $N = 2000$ is $\Delta \gtrsim 600$ meV.

Now let's consider a double-grain system of two bismuth clusters with a point contact. The first cluster with $N_1 \approx 200$ electrons and the second one with $N_2 \approx 2000$. Coupling to the main cluster and interaction with the substrate will destroy the shell structure in the daughter cluster, which is as small as $\sim 3 \times 3 \times 3$ atoms. The resulting spectrum will have a typical inter level spacing $\approx \frac{3}{5} E_{\rm F}/N_1 = 30$ meV (compare to (29)), and all electrons in a smaller cluster with energies $E_{\rm F} \pm 300$ meV will be still localized in a small cluster ($P \sim \delta_1/\Delta \sim 0.1$ - see (28)). It means that for all reasonable biases (less then ± 300 meV) the current transport will go by tunneling through these localized states with discrete spectrum[27].

[27] We assume the following SET geometry: the source lead is connected to a big cluster, and the drain lead to a small one.

The external electric field will polarize this double-grain system, thus shifting these discrete energy levels, and they will give spectral lines in the $\mathrm{d}I/\mathrm{d}V$ plot with a slope different from that of the diamond edges - just like in Fig. 22a.

6.3. Surface States

The double-grain system is, in fact, an unnecessary *ad hoc* hypothesis. As it was shown in the previous section, the shell structure makes a cluster 'nontransparent' for electrons with energies within the gap. The cluster's energy spectrum looks more like a narrow-gap semiconductor than a metal.

For a macroscopic sample, a gap in the spectrum means that for some energies (inside the gap) the Schrödinger equation has no solutions for real values of wave vector k. However, solutions corresponding to complex values of k do exist. If we call k_I the imaginary part of k, the wave function for complex k involves a factor $exp(-k_\mathrm{I}r)$ and, thus, decreases exponentially in one half-space and increases exponentially in the remaining half-space, the limit between both regions being a plane S perpendicular to k_I and defined by the condition $k_\mathrm{I}r = 0$. These solutions are obviously not physically acceptable eigenfunctions for an infinite sample, but, for a semi-infinite sample confined by S, decaying solutions, if they can be matched to decaying waves in vacuum, may become acceptable and give rise to surface states.

The detailed discussion of surface states is beyond the scope of this thesis[28]. Not all results, obtained for a semi-infinite sample, would be directly applicable for a cluster. First of all, there is no fundamental distinction between surface and bulk states for a finite-volume sample. On the other hand, some surface effects should be even stronger in a cluster than in a macroscopic sample. For example, an image potential is stronger for a curved surface than for a plane one, so the image surface states will have a higher binding energy in a cluster[29].

The concrete structure of surface states and their spectrum depends on parameters of the surface barrier and the energy shift of the atomic levels of surface atoms. Computation or even evaluation of these parameters is far beyond the scope of the jellium model. On the other hand, clusters with a few thousands electrons are too large for *ab initio* and molecular-dynamics calculations.

To the best of our knowledge, the surface states in clusters have not been

[28] For further reference one can look in Ref. [51], the most relevant chapters are 5.2.2 (Surface States in Simple Gaps) and 5.8.4 (Image Surface States).

[29] For a plane surface we have an asymptotic potential $\frac{e^2}{4R}$ and for a sphere $\frac{e^2}{R}$.

considered in the literature thus far[30]. Nevertheless, we can put forward some general assertions:

- No other assumptions (like a second grain with a point link) other than the gap in the energy spectrum are required.
- The density of states of surface levels is a factor of $\sim a/D$ less than for bulk states (a is the lattice parameter and D is a cluster diameter). For a bismuth cluster with 400 atoms (2000 electrons) it gives the expected inter level spacing ~ 25 meV, in accordance with experiment.
- As the surface states are localized near the surface (or even at the vacuum side), they are not screened and, thus, are sensitive to an electrostatic field. As a result, an electrostatic perturbation will shift their energies with respect to bulk electrons.

To summarise, the surface state hypothesis seems to explain qualitatively the experimental data most naturally. To make quantitative assertions, a more solid theoretical background is necessary.

6.4. The Things We Can Not Do

It would be nice to demonstrate the shell structure in the grain spectrum directly. The most straightforward idea is to measure a large-scale $I(V)$ curve for bias voltages of a few Δ, where Δ is the gap in the energy spectrum due to the shell formation. Whenever the voltage applied to the main tunneling gap exceeds the next peak in the shell spectrum, there must be a pronounced increase in the tunneling current. Hence, a large-scale $I(V)$ curve will presumably give global information about the grain spectrum even if the distinct energy levels will not be resolved (the latter is questionable at 4 K - see below).

Unfortunately, this is hardly possible for bismuth clusters. The samples become unstable when the bias voltage exceeds some critical value. First, we observed a dramatic increase in switching noise - see Fig. 22c. At higher biases (and at higher gate voltages too) the Coulomb staircases are curved, which implies a non-linear sample capacitance and can be interpreted as sample deformation by electrostatic field. At still higher biases the sample seems to change its shape stepwise - the staircases are discontinuos, and the sample can change its properties (resistance, the phase of gate oscillations, and even

[30] The most relevant publication is Ref. [52], where calculations of Rydberg states for spherical metallic clusters were reported.

the charging energy) irreversibly. The cluster's free energy as a function of deformation is known to have several local minima -see Refs. 16,17. In a strong field a cluster can jump into a new configuration, corresponding to some other local minimum. And there is, of course, an absolute upper limit due to oxide breakdown (about a few Volts).

Thus, the high-voltage spectroscopy data for bismuth clusters look cumbersome and are very difficult to interpret[31]. To extract the shell spectrum from the large-scale $I(V)$ curves, we need more 'rigid' cluster with a stronger ionic contribution into cluster's free energy - see section 7.1.

6.5. The Things We Did

Another trivial idea is to deposit more material to destroy the shell structure. As one can see from (29) one additional atom will not wipe out the shell spectrum. We can (very roughly) estimate how many atoms we have to deposit this way: the effect from n additional electrons will be $\sim \frac{n}{N} E_{\mathrm{F}}$. The shells shall disappear if this parameter will be about the shell gap Δ. On the other hand, the number of shells in a cluster with N electrons is $\sim \sqrt{N}$, i.e. $\Delta \sim E_{\mathrm{F}}/\sqrt{N}$ and so $n \sim \sqrt{N}$. For a bismuth cluster with $N = 2000$ electrons ($400 \approx 7 \times 7 \times 7$ atoms) we need $\sim \sqrt{2000} = 44$ electrons or about 10 atoms, which is equivalent to an additional deposition of 0.2 atomic monolayers.

Looks like it does work this way. As one can see in Fig. 22, an additional deposition of 1 Å wiped out almost all spectral lines (except Coulomb staircases, of course) from the $\mathrm{d}I/\mathrm{d}V$ plot.

Although in the spirit of section 6.2., one can suggest the following interpretation: after additional deposition the contact area between two grains was increased up to 3×3 atoms and the system lost symmetry[32], we believe it is not necessary to assume a double grain system - 1 Å is enough to kill the shells.

What is important in both scenarios, though, is that the newcoming atoms destroy the cluster symmetry, i.e. the cluster did not adjust its shape to find a new absolute free-energy minimum. A perfect cluster shape, resulting in a shell spectrum, is formed only once, presumably in a process of an

[31] The stability region seems to be constrained by Δ itself. Indeed, we can estimate the electrostatic field required to deform a cluster such that the shell structure will be destroyed as $\sim \Delta/D$, where D is cluster diameter. At bias voltage V, the electrostatic field inside the tunneling gap d is V/d, i.e. the critical bias $V \sim \frac{d}{D}\Delta$, the factor $\frac{d}{D}$ being < 1 even for samples with nominal resistance $\sim 10^{10}\Omega$.

[32] As the second cluster was estimated to be $3 \times 3 \times 3$ atoms, it means that both clusters simply joined together.

avalanche reconstruction of the amorphous precursor layer - in accordance with the the mechanism proposed in Ref. [6].

It is still unclear whether it is possible to recover the cluster symmetry by raising the temperature. Above 16 K, the samples start to change their conductance irreversibly. This process eventually leads to widening the tunneling gaps, thus raising the sample resistance above the measurable limit. The only way to recover sample conductivity is to deposit more material, which, in turn, will destroy the cluster symmetry.

On early stages of evolution all samples had some spectral features in the $\mathrm{d}I/\mathrm{d}V$ plot, but after several depositions and/or thermal cycling all spectral lines were wiped out. Of course, even when the grain shape symmetry is broken, the grain spectrum is still quantized. But even for our best sample with charging energy $E_{\mathrm{C}} = 93$ meV an estimated inter-level spacing is ~ 3 meV. The Fermi-distribution of electrons in the leads gives the level smearing $4kT$ (full width at half maximum)[23], or 1.6 meV at 4 K, thus the spectral lines can hardly be resolved at helium temperature.

With the current experimental setup we have to pump out the whole dewar to lower the temperature. Even for temperatures above the λ - point we can keep pumping for a maximum two hours. On the other hand, it took about 50 hours to acquire data presented in Fig. 22. So currently we can not do spectroscopy measurements below helium temperature.

7. FUTURE PLANS: THE THINGS WE CAN TRY

In my dreams
I have a plan ...

AƁBA

7.1. Different Materials

First we can try some other materials. Bismuth is a specific metal, it is superconducting in the quench-condensed amorphous phase and semimetallic in normal crystalline modification. It would be nice to try some simple metal.

As most of theoretical (both analytical and numeric) results were obtained for alkali metals, they may be probably the best choice. Alkali metals are known to form conducting quench-condensed films at extremely low film thicknesses (about one monolayer). So one can expect small clusters and high discrete energy level splitting. Moreover, at a given volume an alkali cluster has less electrons then a bismuth one, as the electron density in alkali metals is substantially lower - compare 14.1×10^{22} cm^{-3} for bismuth (assuming 5 valence electrons per atom) and 0.91×10^{22} cm^{-3} for cesium. For a cesium cluster with charging energy $\sim$ 100 meV an average energy level splitting must exceed 30 meV - well enough for a discrete spectrum to be resolvable at helium temperature.

Another unique advantage of cesium is its low evaporation temperature. By raising the substrate temperature to 300 K it is possible to re-evaporate the cesium film and to clean the substrate for a new deposition cycle. So in one helium experiment the evolution of several samples can be traced[33]. Unfortunately, commercially available cesium sources have either too small capacity or too high power dissipation. We are considering some custom designs, but they were not yet checked.

A challenging goal is to demonstrate a shell spectrum directly from large-scale $\mathrm{d}I/\mathrm{d}V$ measurements, for biases exceeding Δ/e (Δ is the gap in the energy spectrum due to shell formation). Obviously, a cluster shape (and hence an energy spectrum) must not be disturbed much by an applied electric field. For this one needs a 'rigid' cluster, with the ionic component dominating in the cluster's free energy.

One possible material is silver - in contrast to bismuth, silver has no quench-condensed amorphous modification[34]. An extreme case of a 'rigid' cluster is a fullerene molecule, and a fullerene is also easy to evaporate.

[33] If the lead electrodes will not be destroyed by chemically active cesium.
[34] Gold would be even better, but it is too difficult to evaporate.

We can also try some classical superconductor - for example lead. If the shell formation in a lead cluster will result in a gap around the Fermi energy, then the superconductivity in a grain will likely be suppressed. But it is not clean how to detect this effect experimentally.

7.2. Experimental Setup Improvements

An obvious improvement is to arrange a 1 K pot. Hopefully, we will have it working in the next experimental run.

Another crucial step is to re-build a data acquisition setup. Currently, we have at least 2^{14} signal to noise ratio in an analog tract, but only 12-bit AD converters. Although the measurement program samples any data point 16 times, there is no way to reduce quantization error below a certain limit, and it is the discretization error, which dominates in $\mathrm{d}I/\mathrm{d}V$ plots.

Another problem is sweeping the bias with a 12-bit DA-converter. An elementary step in bias current exceeds current noise $\sim$2 fA[35] by one order of magnitude. The bias sweep is therefore not linear, but stepwise. For extremely high-ohmic samples each step in bias current gives a long-term RC-exponent in the time evolution of the voltage signal. This limits the possibility to improve signal to noise ratio by measuring the same data point several times, and puts strong requirements on maximum allowed sampling jitter[36].

An expected effect from upgrading the data acquisition system to a 16-bit resolution is at least ten times signal to noise enhancement. Note that we do need a large dynamic diapason to answer experimentally some obvious questions like, for example, what happens with a discrete energy spectrum when the grain is charged with one extra electron by gate or bias voltage. In large, a voltage scale is given by the Coulomb energy $\sim$ 100 meV, and the finest features in the $\mathrm{d}I/\mathrm{d}V$ curve are as small as $kT \approx 0.1$ meV for 1 K. This gives about $1000 \approx 2^{12}$ significant points in the $\mathrm{d}I/\mathrm{d}V$ curve, which, in turn, requires at least 2^{16} points of $I(V)$ for numeric differentiation.

The most laborious, but the most promising improvement is a few Tesla magnet - see the next section.

[35] An effective current noise on $I(V)$ plots.

[36] An optimum sampling rate is 50 data points per second. As we do 16 AD conversions per data point, the sampling period is 1.25 ms, and sampling jitter must not exceed $(0.1 - 0.2)$ ms, well below the time quanta in PC/Windows environment. To fulfill this requirements we are using a DSP driven data acquisition card with a custom build real time driver.

8. SOME POSSIBLE EFFECTS

They might or they might not,
You never can tell with bees.
Winnie-the-Pooh.

8.1. Possible Effects in a Strong Magnetic Field

A Zeeman shift $\mu_B H$ in magnetic field $H = 10$ T is 0.58 meV (assuming a unity g-factor). On the other hand, the Fermi-distribution of electrons in the leads gives the level smearing $4kT$ (full width at half maximum[23]), or 0.35 meV at 1 K. We can argue, therefore, that a Zeeman shift of energy levels can not be resolved at 1 K, and one should go to dilution refrigerator temperatures. As our samples are metastable, they must be kept at temperatures below (10 - 20) K, and so they must be deposited *in situ*. Even for cesium it is hardly possible to design an evaporator which will operate inside a dilution refrigerator.

At a first glance, it looks rather pessimistic, but we can expect some new effects, which will greatly magnify the energy level shift.

As it was discussed in section 4.3., we have two sets of spectral lines in the $\mathrm{d}I/\mathrm{d}V$ plot - see Fig. 22a on p. 38. The spectral line of the first type, marked by β_i in Fig. 24b on p. 43, appears when the next discrete energy level in a grain spectrum became available for tunneling - see Fig. 26 on p. 45. The spectral line of the second type, marked by γ_i appears when some energy level crosses the chemical potential.

Whereas the typical spacing Δ_β between β-lines in a $\mathrm{d}I/\mathrm{d}V$ plot is determined by an average inter-level spacing in a grain spectrum, the splitting Δ_γ between γ-lines depends also on the sensitivity of discrete energy levels ξ_i to an electrostatic field E:

$$\Delta_\gamma = \Delta_\beta / K,$$

where $K \sim \mathrm{d}\xi/\mathrm{d}E$. We can estimate K from Fig. 22a to be ~ 5.

If this scenario is correct, then the shift in a magnetic field for lines of type γ must be the same factor K stronger than for β-lines. An experimental observation of the anomalous g-factor for γ-lines will be a strong support in favor of the proposed mechanism.

There is one more reason to expect an anomalous sensitivity of the grain spectrum to magnetic field. The ground state of a cluster with a partially filled shell is expected to be spin-polarized - see Refs. [18,19]. An expected spontaneous spin is about the number of electrons in the outermost unfilled

shell, i.e. $\sim \sqrt{N}$ for a cluster with N electrons. If this is the case, then the grain must be *mechanically* deformed by a magnetic field.

Measuring the tunneling resistance we can detect extremely small grain deformations - $\sim (0.1 - 0.01)$ Å. An experimental observation of the SET conductance sensitivity to magnetic field will complement the temperature dependence observed in Ref. [54], and will further support the idea that the quench-condensed clusters are "soft", and their shape is sensitive to mechanical perturbations.

On the other hand, if a cluster *is* deformed in magnetic field, then the quantized energy levels will be shifted due to cluster deformation. This is a cooperative effect, and it can manyfold exceed the Zeeman shift. So, in principle, we can expect an anomalous giant g-factor even for orthodox spectral lines.

8.2. The Temperature Dependence of the Cluster Spectrum

A unique phase transition for open shell clusters was predicted theoretically in Ref. [15] and, we believe, was observed for our samples - see section 2. At zero temperature the cluster is deformed due to spontaneous distortion of the ground state. At some critical temperature the thermal motion of the cluster atoms recovers the spherical symmetry. There is a high-order phase transition associated with this scenario, where the cluster shape plays the role of the order parameter. It means that a distortion η as a function of temperature near the transition point T_c has a singular behaviour (see Ref. [55]):

$$\begin{aligned} \eta(T) &= \left(1 - \frac{T}{T_c}\right)^{\nu} \quad \text{for } T < T_c; \\ \eta(T) &= 0 \qquad\qquad\quad \text{for } T > T_c. \end{aligned} \tag{31}$$

As the cluster distortion shifts the energy levels ξ_i in a grain spectrum, the same dependency must be observed for $\xi_i(T)$. An expected effect is sketched in Fig. 33. An observation of this effect will be the *direct* confirmation of the existence of a phase transition in a grain.

An open question is the fluctuation region δT near T_c. On one hand, this is a transition in an electronic system, so on can expect $\delta T/T_c \ll 1$, like, for example, in a superconducting transition. But, on the other hand, the electron-electron and electron-ion interactions in a cluster are non-separable (Ref. [15]), and the ionic subsystem is also involved in the transition. As a result, the fluctuation region can be rather wide. This can lead to smeared spectral lines, and will probably make them unresolvable [37].

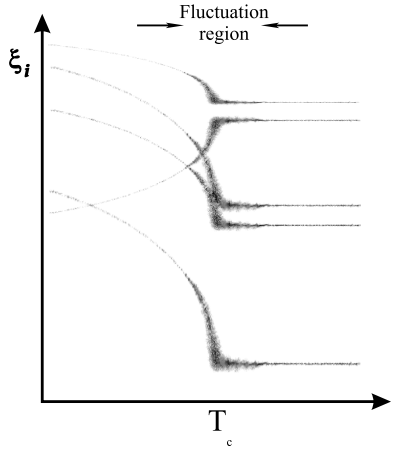

Fig. 33. An expected temperature dependence of discrete energy levels ξ_i in cluster.

[37] Compare with the width of the single-electron excitations due to mechanical quadrupole and monopole oscillations estimated in Ref. [16], Appendix C.

9. CONCLUSIONS

The assumption of Coulomb blockade is rather dubious.
APL Referee for Ref. [8]
The interpretation of the results is however rather speculative.
PRL Referee B for Ref. [54].

- We have developed a new method based on the combination of angle deposition through an electron-beam defined shadow mask and *in situ* conductance measurements. The first implementation of this method resulted in a room-temperature operating SET. At helium temperatures this method allows to isolate a *single* cluster in a quench-condensed film and to fabricate, in a controllable way, a SET transistors with charging energies up to 100 meV.

- For SET transistors built around a cluster of quench-condensed bismuth a remarkable reversible manyfold increase of current was found as the temperature was lowered below ~ 7 K. This effect is attributed to a phase transition of a new type, with a cluster shape as the order parameter. At zero temperature the cluster is deformed due to spontaneous distortion of the ground state, and above the transition temperature the thermal motion of the cluster atoms recovers the spherical symmetry.

- Preliminary spectroscopy measurements on quench-condensed bismuth clusters in a well-defined SET geometry were performed. The spectroscopy data can be interpreted in the frame of a two-liquid model with two different electron communities in a grain:

  - Electrons from the first group do not contribute noticeably into current transport, but they form a majority of quantum states in the grain and define the chemical potential.
  - Electrons from the second group dominate in transport. Their energy levels are shifted by electrostatic perturbation with respect to a chemical potential, fixed by electrons from the first group.

- Two most realistic implementations of two-liquid model:

  - the double grain system with an atomic-size contact
    and
  - the surface-localized electron states in a cluster

  both exploit the assumption that there is a gap in the energy density of states near the Fermi energy due to formation of a shell structure in the cluster spectrum.

To summarize, an anomalous temperature dependence and non-orthodox SET tunneling spectra can be understood if the shell structure is indeed formed in quench condensed clusters. This implies that the electronic subsystem governs the cluster shape. The cluster is not frozen: its shape and its energy spectrum is sensitive to electrostatic and thermal perturbations. The energy gap in a shell spectrum makes the electronic properties of a cluster rather different from these of a bulk metal.

ACKNOWLEDGEMENTS

I would like to thank my examiner, Prof. Lars Wallden and my supervisor Prof. Håkan Olin for providing me an opportunity to participate in this research program. I would like to thank as well Prof. Tord Claeson for guidance and critical reading this manuscript.

All experimental work discussed in this thesis was done together with Sergey Kubatkin.

Help and fruitful discussions from Dmitri Golubev, Alexander Tzalenchuk, August Yurgens, Robert Shekhter, Leonid Gorelik and many other people are gratefully acknowledged.

Our experiments would not have run without the help of Staffan Pehrson and Rune Söderlund.

Special thanks to Ann-Marie Frykestig and Ingrid Riedl for all help with administrative stuff.

REFERENCES

1. R.C. Dynes, J.P. Garno, J.M. Rowell, *Phys. Rev. Lett.* **40**, 479 (1978).
2. G. Bergmann, *Phys. Rep.* **107**, 1 (1984).
3. M.Strongin, *Phys. Rev. B* **1**, 1078, (1970); R.C. Dynes, A.E. White, J.M. Graybeal, J.P. Garno, *Phys. Rev. Lett.* **57**, 2195 (1986); H.M. Jaeger, D.B. Haviland, B.G. Orr, A.M. Goldman, *Phys. Rev. B* **40**, 182 (1989); I.L. Landau, D.L. Shapovalov, I.A. Parshin, *JETP Lett.* **53**, 5 (1991).
4. A.V. Danilov, S.E. Kubatkin, I.L. Landau, I.A. Parshin, L. Rinderer, *Phys. Rev. B* **51**, 5514 (1995).
5. A.V. Danilov, S.E. Kubatkin, I.L. Landau, L. Rinderer, *J. Low Temp. Phys.* **103**, 35 (1996).
6. K.L. Ekinchi, J.M. Valles, Jr., *Phys. Rev. B* **58**, 7347 (1998); K.L. Ekinchi, J.M. Valles, Jr., *Phys. Rev. Lett.* **82**, 1518 (1999).
7. S.E. Kubatkin, A.V. Danilov, A. Bogdanov, H. Olin, T. Claeson, *Journ. of Surf. Analysis* **4**, 235 (1998). Appended paper #**1**.
8. S.E. Kubatkin, A.V. Danilov, A.L. Bogdanov, H. Olin, T. Claeson, *Appl. Phys. Lett.* **73**, 3604 (1998). Appended paper #**2**.
9. S.E. Kubatkin, A.V. Danilov, H. Olin, T. Claeson, to appear in *Physica B.* Appended paper #**3**.
10. S.E. Kubatkin, A.V. Danilov, H. Olin, T. Claeson, to appear in *Journ. of Low Temp. Phys.*. Appended paper #**4**.
11. D.V. Averin, K.K. Likharev, in *Mesoscopic Phenomena in Solids*, (North-Holland, New York, 1991), Chap. 6.
12. D.V. Averin, A. N. Korotkov, K.K. Likharev, *Phys. Rev. B* **44**, 6199 (1991).
13. A.T. Johnson, L.P. Kouwenhowen, W. de Jong, N.C. van der Vaart, C.J.P.M. Harmans, C.T. Foxon, *Phys. Rev. Lett.* **69**, 1592 (1992).
14. N.W. Ashcroft, N.D. Mermin, *Solid State Physics*, (Holt, Rinehart & Winston, New York, 1996).
15. V.M. Akulin, C. Bréchignac, A. Sarfati, *Phys. Rev. Lett.* **75**, 220 (1995).
16. W.A. de Heer, *Rev. Mod. Phys.* **65**, 611 (1993).
17. M. Brack, *ibid*, 677.
18. M. Tinkham, D. Davidović, D.C. Ralph, C.T. Black, to appear in *Journ. of Low Temp. Phys.*
19. L.I. Glasman, to appear in *Journ. of Low Temp. Phys.*
20. A.I. Yanson, I.K. Yanson, J.M. van Ruitenbeek, *Nature* **400**, 144 (1999).
21. A. Bulgac, C. Lewenkopf, *Phys. Rev. Lett.* **71**, 4130 (1993).
22. L.D. Landau, E.M. Lifshitz, *Statistical Physics; Part 1*, (Pergamon Press, New York, 1989), Vol. 5, Chap. XIV, §144.
23. D. Davidović, M. Tinkham, *cond-mat/* **9905043**, (1999).
24. R. C. Ashoori, *Nature* **379**, 413 (1996).
25. M. A. Kastner, *Phys. Today* **1**, 24 (1993).
26. H. van Houten, C.W.J. Beenakker, A.A.M. Staring in *Single Charge Tunneling*, (Plenum Press, New York, 1992), Chap. 5.
27. S. Tarucha, D.G. Austing, T. Honda, R.J. van der Hage, L.P. Kouwenhoven, *Phys. Rev. Lett.* **77**, 3613 (1996).
28. L.P. Kouwenhoven, T.H. Oosterkamp, S. Tarucha, D.G. Austing, T. Honda

Physica B **249-251**, 191 (1998).
29. L.P. Kouwenhoven, T.H. Oosterkamp, M.W.S. Danoesastro, M. Eto, D.G. Austing, T. Honda, S. Tarucha, *Science* **278**, 1788 (1997).
30. T.H. Oosterkamp, S.F. Godijn, M.J. Uilenreef, Y.V. Nazarov, N.C. van der Vaart, L.P. Kouwenhoven, *Phys. Rev. Lett.* **80**, 4951 (1998).
31. D.G. Austing, T. Honda, K. Muraki, Y. Tokura, S. Tarucha, *Physica B* **249-251**, 206 (1998).
32. D.C. Ralph, C.T. Black, M. Tinkham, *Phys. Rev. Lett.* **74**, 3241 (1995).
33. D.C. Ralph, C.T. Black, M. Tinkham, *Phys. Rev. Lett.* **78**, 4087 (1997).
34. D.L. Klein, A.K.L. Lim, A.P. Alivisatos, P.L. McEuen, *Nature* **389**, 699 (1997).
35. E. Braun, Y. Eichen, U. Sivan, G. Ben-Yoseph, *Nature* **391**, 775 (1998).
36. S.H.M. Persson, L.G.M. Olofsson, L.K. Gunnarsson, *Appl. Phys. Lett.* **74**, 2546 (1999).
37. L.G.M. Olofsson, S.H.M. Persson, A. Morpurgo, C.M. Marcus, D. Golubev, L.K. Gunnarsson, Y. Yao, to appear in *Journ. Low Temp. Phys.*
38. A.M. Clogston, *Phys. Rev. Lett.* **9**, 266 (1962); B.S. Chandrasekhar, *Appl. Phys. Lett.* **1**, 7 (1962).
39. F. Braun, J. von Delft, D.C. Ralph, M. Tinkham, *Phys. Rev. Lett.* **79**, 921 (1997).
40. Yu.A. Pashkin, Y. Nakamura, J.S. Tsai, submitted to *Appl. Phys. Lett.*
41. W. Chen, H. Ahmed, K. Nakazoto, *Appl. Phys. Lett.* **66**, 3383 (1995).
42. E. Leobandung, L. Guo, Yu. Wang, S. Chou, *Appl. Phys. Lett.* **67**, 938 (1995).
43. H. Ishikuro, T. Fujii, T. Saraya, G. Hashiguchi, T. Hiramoto, T. Ikoma, *Appl. Phys. Lett.* **68**, 3585 (1996).
44. I. M. Ruzin, V. Chandrasekhar, E. I. Levin, and L. I. Glasman, *Phys. Rev. B* **45**, 13469 (1992).
45. M. Kemerink and L. W. Molenkamp, *Appl. Phys. Lett.* **65**, 1012 (1994).
46. O. Agam, N.S. Wingreen, B.L. Altshuler, D.C. Ralph, M. Tinkham, *Phys. Rev. Lett.* **78**, 1956 (1997).
47. B.L. Altshuler, Yu. Gefen, A. Kamenev, L.S. Levitov, *Phys. Rev. Lett.* **78**, 2803 (1997).
48. D. Davidović, M. Tinkham, *Phys. Rev. Lett.* **83**, 1644 (1999).
49. N.C. van der Vaart, A.T. Johnson, L.P. Kouwenhowen, D.J. Maas, W. de Jong, M.P. de Ruyter van Steveninck, A. van der Enden, C.J.P.M. Harmans, C.T. Foxon, *Physica B*, **189**, 99 (1983).
50. C. Bréchignac, Ph. Cahusac, F. Carlier, M. de Frutos, J.Ph. Roux, *Phys. Rev. B* **47**, 2271 (1993).
51. M.C. Desjonquéres, D. Spanjaard, *Concepts in Surface Physics*, (Springer, New York, 1996).
52. J-P Connerade, A. Ipatov, *J. Phys. B* **31**, 2429 (1998).
53. M.H. Devoret, D. Esteve, H. Grabert, G.-L. Ingold, H. Pothier, C. Urbina, in *10 Years of STM*, (North-Holland, New York, 1992), p. 22.
54. S.E. Kubatkin, A.V. Danilov, H. Olin, T. Claeson, submitted to *Phys. Rev. Lett.*
55. Shang-Keng Ma, Modern theory of critical phenomena, (Addison-Wesley, New-York, 1976), Chap. I.3, p. 10.

LIST OF APPENDED PAPERS

Two papers in one week, not one paper in five years!
Håkan Olin.

- **1.** S.E. Kubatkin, A.V. Danilov, A. Bogdanov, H. Olin, T. Claeson, Room temperature SET effects in nano-constricted granular films. *Journ. of Surf. Analysis* **4**, 235 (1998).

- **2.** S.E. Kubatkin, A.V. Danilov, A.L. Bogdanov, H. Olin, T. Claeson, Coulomb blockade effects at room temperature in thin-film nanoconstrictions fabricated by a novel technique. *Appl. Phys. Lett.* **73**, 3604 (1998).

- **3.** S.E. Kubatkin, A.V. Danilov, H. Olin, T. Claeson, Anomalous Coulomb blockade in nanoconstricted quench-condensed Bi films. To appear in *Physica B*.

- **4.** S.E. Kubatkin, A.V. Danilov, H. Olin, T. Claeson, Tunneling through a single quench-condensed cluster. To appear in *Journ. of Low Temp. Phys.*

- **5.** APPENDIX A. Single Electron Tunneling.

Appended paper 1.

Appended paper 2.

Appended paper 3.

Appended paper 4.

APPENDIX A.